remote sensing

MDPI

Article

Multi-Decadal Trends in Aerosol Optical Depth of the Main Aerosol Species Based on MERRA-2 Reanalysis: A Case Study in the Baltic Sea Basin

Enrico Mancinelli [1], Giorgio Passerini [2], Simone Virgili [2] and Umberto Rizza [3,*]

[1] Department of Pure and Applied Sciences, University of Urbino, 61029 Urbino, Italy
[2] Department of Industrial Engineering and Mathematical Sciences, Marche Polytechnic University, 60131 Ancona, Italy
[3] Institute of Atmospheric Sciences and Climate, National Research Council, 73100 Lecce, Italy
* Correspondence: umberto.rizza@cnr.it

Abstract: This study analyses the trends of total aerosol and the main aerosol species over nine capitals in the Baltic Sea basin from 1989 to 2019 based on the Modern-Era Retrospective Analysis for Research and Applications, Version 2 Reanalysis. Aerosol speciation includes mineral dust, sea salt, sulphate (SO_4), organic carbon (OC), and black carbon (BC). The mean total aerosol optical depth (AOD) values were the highest (up to 0.216) over the continental capitals (i.e., Warsaw, Berlin, and Vilnius). For each capital, the mean SO_4 AOD was the main aerosol species, with a trend specular to total AOD. Apart from Warsaw, the mean BC AOD was the aerosol species with the lowest level. The composition of aerosols changed with respect to the species of anthropogenic origins (i.e., SO_4, OC, and BC), with the percentage contribution to the total AOD decreasing for the SO_4 AOD and increasing for the BC AOD. Also, the OC AOD showed an increase in the percentage contribution to total AOD for Copenhagen, Oslo, Stockholm, and the continental capitals. Anthropogenic aerosols contributed up to 90.3% of the total AOD, with the highest values over the continental capitals. For each capital, the minimum in the percentage contribution of anthropogenic AOD was between 2007 and 2008, likely due to the global financial crisis. Anthropogenic AOD as a percentage of the total AOD decreased from 1989 to 2008. Both the total and the SO_4 AODs decreased over each capital. By contrast, the BC AOD increased over Stockholm, and both the OC and BC AODs increased over Berlin, Copenhagen, and Oslo. The decoupling of carbonaceous aerosols and the SO_4 AOD trends was likely due to concurrent factors such as biomass burning and low-sulphur fuel policies. From 2000 to 2019, the inverse relationships between gross domestic products and SO_4 AODs suggest a relative decoupling of economic growth from fossil fuels for Oslo, Stockholm, Tallinn, and Vilnius.

Keywords: AOD; MERRA-2; urban air pollution; proxies; aerosol speciation; anthropogenic; natural; Europe

Citation: Mancinelli, E.; Passerini, G.; Virgili, S.; Rizza, U. Multi-Decadal Trends in Aerosol Optical Depth of the Main Aerosol Species Based on MERRA-2 Reanalysis: A Case Study in the Baltic Sea Basin. *Remote Sens.* **2024**, *16*, 2421. https://doi.org/10.3390/rs16132421

Academic Editor: Carmine Serio

Received: 10 May 2024
Revised: 24 June 2024
Accepted: 26 June 2024
Published: 1 July 2024

1. Introduction

Aerosol optical depth (AOD) is a unitless measure of the interaction of solid or liquid airborne particles with sunlight in the air column. In this context, it may be considered a proxy for the level of atmospheric pollution.

Previous air-quality studies observed negative AOD trends over the most populated European cities, the European continent, or certain areas within Europe based on AOD reanalysis [1,2] satellite measurements [3–7] or datasets from multiplatform observations and reanalysis [8,9] in the time span of the last two decades. Mehta et al. [3] reported negative AOD trends for total AOD, and polluted dust and smoke AODs associated with negative aerosol extinction trends up to 2 km above sea mean level based on ten-year-long CALIOP (Cloud Aerosol Lidar with Orthogonal Polarization; [10] observations. Gupta et al. [11] ascribed the decreasing total AOD trend to decreasing SO_4 and dust AODs

based on the MERRA-2 (Modern-Era Retrospective Analysis for Research and Applications, Version 2; [12]), and to a decrease in dust, polluted dust, and elevated smoke in the free troposphere based on CALIOP over Europe. Based on the MERRA [13] reanalysis, Provençal et al. [1] analysed AOD aerosol species and trends over the most populated cities in the world over a 13-year period from 2003 to 2015. These authors observed a general decrease in both total and SO_4 AODs for a selection of capitals in Europe.

Several authors [3,4,8,9] suggested that decreasing trends in annual mean AOD levels were attributable to the enforcement of environmental regulations aimed at decreasing emissions of NO_X and SO_X, or a shift to a greener energy mix [14] in Europe. According to Naqvi [15], the EU regions with the highest income per capita showed a lower responsiveness to environmental regulations, varying with the emission types, likely due to a shift towards the service sector.

Previous studies [1,16] reported relationships between variations in economic, industrial, and energy indicators, the levels of anthropogenic aerosol load, and the relative contribution to total aerosol.

Papachristopoulou et al. [17] investigated the AOD variability of 81 world megacities' urban agglomerations and their respective surrounding areas based on spatial gradient analysis. According to these authors, about 65% of megacities showed higher 18-year mean AOD values over the city's centre compared to the surrounding areas. Di Antonio et al. [7] analysed the variation in local and regional AOD levels based on the MAIAC (Multi-Angle Implementation of Atmospheric Correction; [18]) algorithm applied to MODIS (Moderate Resolution Imaging Spectroradiometer; [19,20]) observations from 2000 to 2021 over several cities in Europe. According to these authors, local AOD levels in European cities such as Paris, Athens, and Barcelona were higher compared to the regional AOD levels because of the contributions of local anthropogenic emissions and favourable atmospheric conditions.

No studies have investigated the AOD aerosol species over the Baltic Sea area for a time span longer than 20 years. To fill this gap in AOD studies, we investigated the trends of total aerosol and aerosol species over the capitals of 9 countries in the Baltic Sea basin, namely Denmark, Estonia, Finland, Germany, Latvia, Lithuania, Norway, Poland, and Sweden from 1989 to 2019 based on MERRA-2 reanalysis. In this time span, drastic changes occurred in the Baltic area in the socioeconomic, political, and historical spheres. In this context, following the collapse of the Soviet Union, the Baltic states, Germany, and Poland made significant reforms in their economic and political systems.

2. Materials and Methods

2.1. Study Region: Economic, Population and Energy Statistics

Figure 1 shows the location of the study area, the countries, and the capitals in the Baltic Sea basin. Based on the location, the capitals can be grouped as continental (Berlin, Warsaw, and Vilnius) and coastal cities (Copenhagen, Helsinki, Oslo, Riga, Stockholm, and Tallinn) (Figure 1b).

Annual data at the national level (NUTS1, the nomenclature of territorial units for statistics level 1 [21]) and the local level (NUTS3) were retrieved from the EUROSTAT database (https://ec.europa.eu/eurostat/data/database, accessed on 22 January 2023). Preference was given to the data with the finest geographical resolution (i.e., NUTS3). Data about energy efficiency and the share of fossil fuel in the gross available energy (SFFGAE) were only available at NUTS1 level.

At the NUTS3 level, Berlin was the most populated, followed by Helsinki, Warsaw, and Stockholm with populations in the range 1.2–2.3 million people. The other statistical entities had populations in the range 530–850 thousand people (Figure 2a). In the last decades, an increase in population occurred in Berlin, Helsinki, Copenhagen, and Oslo, whereas Riga and Vilnius showed a decreasing trend in population.

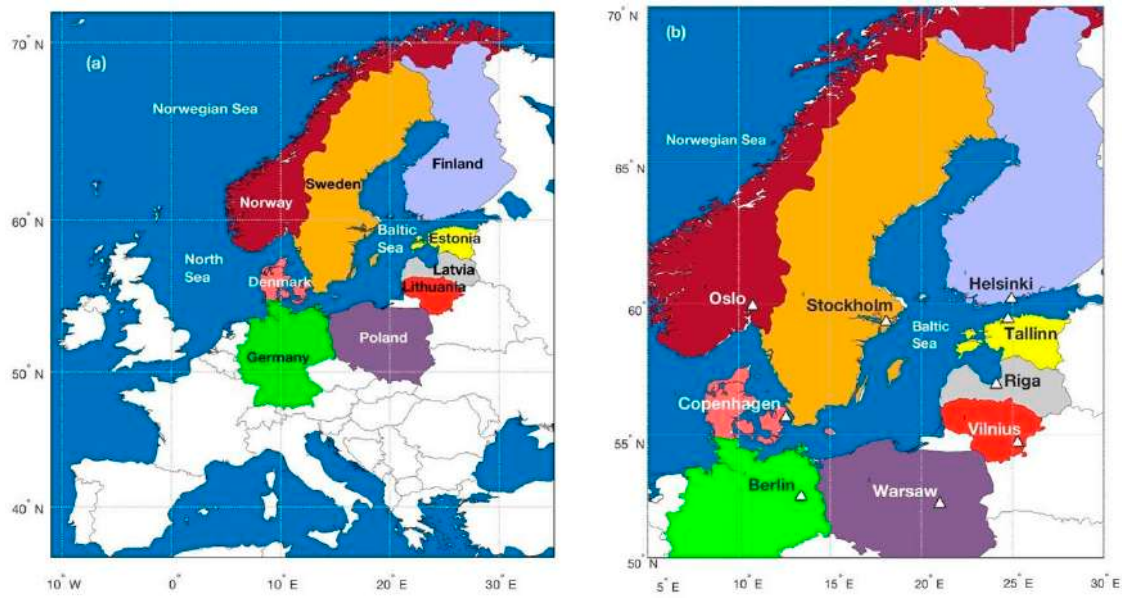

Figure 1. Location of (**a**) the study area in Europe, and (**b**) the capitals of countries in the Baltic Sea basin.

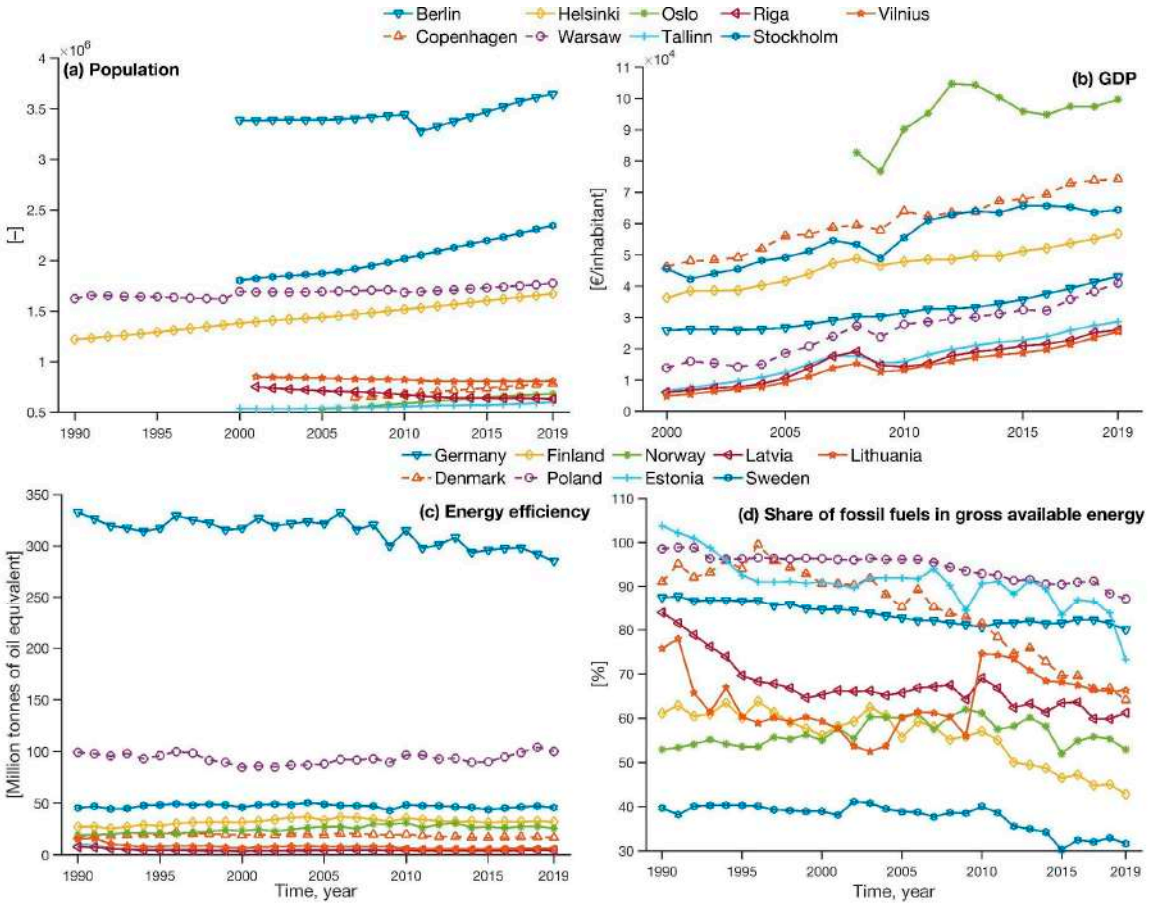

Figure 2. Population (**a**) and gross domestic product (GDP) (**b**) at nomenclature of territorial units for statistics (NUTS) 3 level, energy efficiency (**c**), and share of fossil fuels in gross available energy (**d**) at NUTS1 level in the Baltic Sea basin. This is our own elaboration based on data from EUROSTAT (https://ec.europa.eu/eurostat, accessed on 22 January 2023).

At the NUTS3 level, the mean gross domestic product (GDP) per capita was the highest for Oslo (about EUR 95 thousand per capita), followed by Copenhagen, Stockholm, and Helsinki with values in the range EUR 47–61 thousand per capita, Berlin and Warsaw (EUR 32 and 26 thousand per capita, respectively), and Riga, Vilnius, and Tallinn (EUR 14–17 thousand per capita) (Figure 2b). With the economic crisis of 2008–2009, all the statistical entities except for Berlin showed lower GDPs. Despite the economic crisis, the GDPs had a similar increasing trend from 2000 to 2019 for all the statistical entities except for Oslo, which had a steady increase between 2009 and 2012, but a shorter time series.

At the national level, primary energy consumption was the highest in Germany, which had about three times the primary energy consumption in Poland, which in turn was more than twice the primary energy consumption of the other countries between 1990 and 2019 (Figure 2c).

The highest values of SFFGAE (52.5–103.8%) were in Germany, Poland, Denmark, Estonia, Latvia, and Lithuania, whereas the lowest values (30.3–63.8%) were in Finland, Sweden, and Norway. All of the countries except for Lithuania and Norway showed a decreasing trend in SFFGAE. In 2010, the shutdown of a nuclear power plant led to a steady increase in SFFGAE in Lithuania. This nuclear power plant was designed to provide about 40% of the power consumption of the Baltic states [22]. However, between 2004 and 2012, the increases in emissions per capita were due to increases in economic activity for the Baltic States and to variations in the energy mix only for Lithuania [23].

We considered energy statistics (energy efficiency and SFFGAE), and GDP per capita (Table A1) to be proxies of anthropogenic activities related to emissions. Therefore, we investigated these indicators as potential predictors of the AOD in the atmosphere over each city, specifically the anthropogenic AOD of aerosol components.

2.2. MERRA-2

MERRA-2 [12] was introduced to replace the original MERRA reanalysis because of the advances made in the assimilation system (https://gmao.gsfc.nasa.gov/reanalysis/MERRA-2/, accessed on 4 September 2023). Table 1 synthesises the MERRA-2's main features. The MERRA-2 dataset covers the period 1980 to present with assimilations of both aerosol and meteorological observations. For the assimilation of meteorological observations, MERRA-2 is based on the Goddard Earth Observing System (GEOS-5) version 5.12.4, comprising the GEOS atmospheric model [24,25], the grid point statistical interpolation analysis system [26,27], and a horizontal discretisation on the cubed sphere grid by Putman and Lin [28]. The horizontal resolution is $0.5^\circ \times 0.625^\circ$.

The Goddard chemistry, aerosol, radiation, and transport (GOCART) model [29,30] is integrated into the GEOS atmospheric model of the emission, sink, and chemistry of the main aerosol species, with specialised modules for emissions, chemistry, advection, planetary boundary-layer turbulent mixing, dry and wet depositions, and moist convection. The GOCART model assumes external mixing with no interactions of the different aerosol species [29]. GOCART speciation includes mineral dust (DU), sea salt (SS), sulphate (SO_4), hydrophobic and hydrophilic organic carbon (OC), and black carbon (BC).

MERRA-2 assimilates bias-corrected AOD observations from the spaceborne Advanced Very High Resolution Radiometer (AVHRR; 1979–2002; [31]), MODIS on Terra 2000–present, and Aqua 2002–present [19,20], the Multiangle Imaging Spectro Radiometer (MISR; 2000–2014; [32]) and the ground-based Aerosol Robotics Network (AERONET; 1999–2014; [33]).

The annual mean total AOD and speciated AODs at 550 nm were also used for this study.

Table 1. Resume of the MERRA-2 main features adapted from Lacima et al. [34].

Coverage period	1980–present
Spatial resolution	0.5° × 0.625° (∼50 km)
Assimilation system	3DVar Gridpoint Statistical Interpolation [26,27]
Meteorology	GEOS-5 [24,25]
Chemistry	GOCART [29,30]
Anthropogenic emissions	AeroCom Phase II (HCA0 v1; [35]), EDGARv4.2 [36,37]
Biomass burning emissions	RETRO v2 [38], GFEDv3.1 [39,40], QFED 2.4-r6 [41]
Biogenic emissions	Biogenic non-methane volatile organic compounds [42]
Volcanic emissions	AeroCom Phase II (HCA0 v2; [35])
Assimilated aerosol products	AVHRR, AERONET, MISR, MODIS

Methodology for Emission Sources in MERRA-2

In MERRA-2 the AOD at 550 nm is the only property directly constrained by the data assimilation system if AOD observations are available. Aerosol speciation is indirectly constrained by this assimilation and strongly controlled by lower boundary conditions (i.e., emissions inventories) [43], the parameterisation of the model's physics, and error covariance assumptions [12]. Gupta et al. [8] reported high correlation values (above 0.6) between the MERRA-2 and AERONET AOD datasets between 2001 and 2020 around the world. Randles et al. [44] pointed out that trends of both the total and the main aerosol species AODs may be affected by data availability and coverage, and changes in the observing system or the emissions inventories.

For the GOCART model [29,30], the authors set the height of emissions depending on the types of sources. Specifically, emissions of dust and sea salt come from surface sources. Anthropogenic emissions occur above or below 100 m. Biomass burning emissions are evenly distributed in the planetary boundary layer with respect to the grid cells where the biomass burning occurred. Volcanic emissions are modelled according to the magnitude of the eruption and the altitude of the volcano.

Anthropogenic emissions of SO_2 are based on the Emissions Database for Global Atmospheric Research (EDGAR), Version 4.3.2 database [45] updated until 2012 and repeated in MERRA-2 in the following years. The AeroCom Phase II dataset (HCA0 v1) [35] provides anthropogenic emissions of OC, BC, and primary SO_4 aerosols, including aircraft SO_2 emissions. AeroCom Phase II was updated until 2006. Emissions of OC, BC, and SO_4 aerosols from oceangoing vessels are drawn from a database compiled by Eyring et al. [46] and updated until 2007.

It is important to point out that MERRA-2 repeats the emissions recorded in the databases (e.g., EDGAR version 4.3.2 [45], AeroCom Phase II [35]) to account for the years when those databases were no longer bring updated [44]. Lacima et al. [34] reported an increasing overestimation of surface concentrations of SO_2 from the MERRA-2 reanalysis compared to measured surface concentrations from monitoring stations on the European continent from 2003 to 2020. These authors suggested that this bias may arise from the last available update of the MERRA-2 anthropogenic SO_2 emission databases (i.e., AeroCom Phase II and EDGAR 4.3.2) and propagate until the next emission inventory updates.

Both dust and sea salt emission schemes are wind-dependent. Dust emissions depend on soil size distribution, the roughness lengths, and the threshold wind friction velocity as described in Marticorena and Bergametti [47]. The sea salt emission scheme is parameterised according to Gong [48] and corrected considering the dependency of the emissions on sea surface temperature as described in the work by Jaeglé et al. [49].

The emission of biogenic non-methane volatile organic compounds varies with solar radiation and temperature depending on the ecosystems and the plant types [42].

Estimates of the emissions resulting from biomass burning are based on different databases depending on the time frame between 1980 and the present. From 1980 to 1996, the monthly mean biomass burning emissions of carbonaceous aerosol and SO_2 relies on RETROv2 emissions [38]) based on an aerosol index derived from TOMS (Total Ozone Mapping Spectrometer; [50]), and fire data from AVHRR and ATSR (Along Track Scanning Radiometers; [51]). For biomass burning emissions between 1997 and 2009, MERRA-2 relies on the Global Fire Emissions Database (GFED), Version 3.1 [39,40], which is based on satellite data and a biogeochemical model. Starting from 2010, the estimates of the daily mean emissions of carbonaceous aerosol, SO_2, CO, and CO_2 from biomass burning are based on the Quick Fire Emissions Dataset (QFED) version 2.4-r6 [41], with fire radiative power data and the locations of fires drawn from MODIS [52].

Daily volcanic emissions of SO_2 both from eruptive and degassing volcanoes are based on the AEROsol COMparisons between Observations and Models (AeroCom) Phase II project data [35] gathered from 1979 to 2010. From 2010 forward, only degassing volcanoes are considered. No eruptive volcanoes are included in the data after 2009.

Considering the 1989–2012 period, emissions of SO_2, NO_X, CO, and $PM_{2.5}$ decreased in 28 EU countries, according to EDGAR v4.3.2 [45].

2.3. MODIS and MISR

The MODIS sensors aboard the Terra and Aqua satellites provide a near-daily global coverage on a $1^\circ \times 1^\circ$ grid, using 36 spectral bands in the range of 410–15,000 nm and a 2330 km screening swath [53]. For MODIS sensors, the Deep Blue algorithm retrieves aerosols over bright surfaces including urban areas at 412 and 470 nm [54]. AOD is measured over dark surfaces (ocean and vegetated lands) through the Dark Target algorithm [20,55]. The merged Dark Target and Deep Blue AOD dataset allows us to extend the spatial coverage of these two algorithms [56]. For this study, we considered the monthly Level-3 MODIS combined Dark Target and Deep Blue AOD at 550 nm, which was collected from the Terra satellite. The MISR instrument aboard the Terra spacecraft provides global coverage data every nine days for a spatial resolution of up to 275 m through nine discrete cameras spanning from 0 to 70.5 degrees in the forward and backward directions, and it uses the 555 nm retrieval wavelengths for AOD measurements [57].

Depending on the sensors, different time spans were available for comparisons with annual mean total AODs from MERRA-2. Specifically, annual mean total AODs were available for the time ranges 2001–2019 and 2001–2017 from MODIS and MISR, respectively.

2.4. Statistical Analysis and Calculations

For describing the response variables (i.e., the annual mean total and SO_4 AODs), we considered the following potential predictive variables: annual data of GDP, energy efficiency, and SFFGAE. Stepwise linear regression was used to select the predictive variables most significant in explaining the total and SO_4 AOD datasets as previously presented in a work by Mancinelli et al. [58]. This method considers the selected predictive variables depending on their statistical significance in explaining the response variables through an iteration of multiple regressions [59]. Specifically, an initial model is replaced by the new starting model if the new model fits the dataset with a constant and a predictive variable with a p-value below the threshold [60]. A term is added to the model for a p-value below 0.05 because this allows us to reject the null hypothesis that the term would have a zero coefficient if added to the model. A term is removed from the model for a p-value above 0.1 because this allows us to accept the null hypothesis that the term has a zero coefficient. The coefficient of determination (R^2) spans between 0 and 1, with higher R^2 values if more variability in the response variable is explained by the predictive variables.

In Figure 2, it is evident that the data of the predictive variables are sparse and do not cover the entire study period (i.e., 1989–2019). Therefore, we considered the time from 2000 to 2019 for all the capitals apart from the capitals with predictive variables available for a shorter time span [i.e., Oslo (2005–2019) and Copenhagen (2007–2019)].

3. Results

3.1. Spatial Distribution of Anomalies in Sulphur Oxides, Organic, and Black Carbon Emissions from MERRA-2 Database between 2019 and 1989–2018

The emissions anomalies of SO_X, OC, and BC were calculated between 2019 and 1989–2018 for the study domain based on the MERRA-2 emissions database (Figures 3–5).

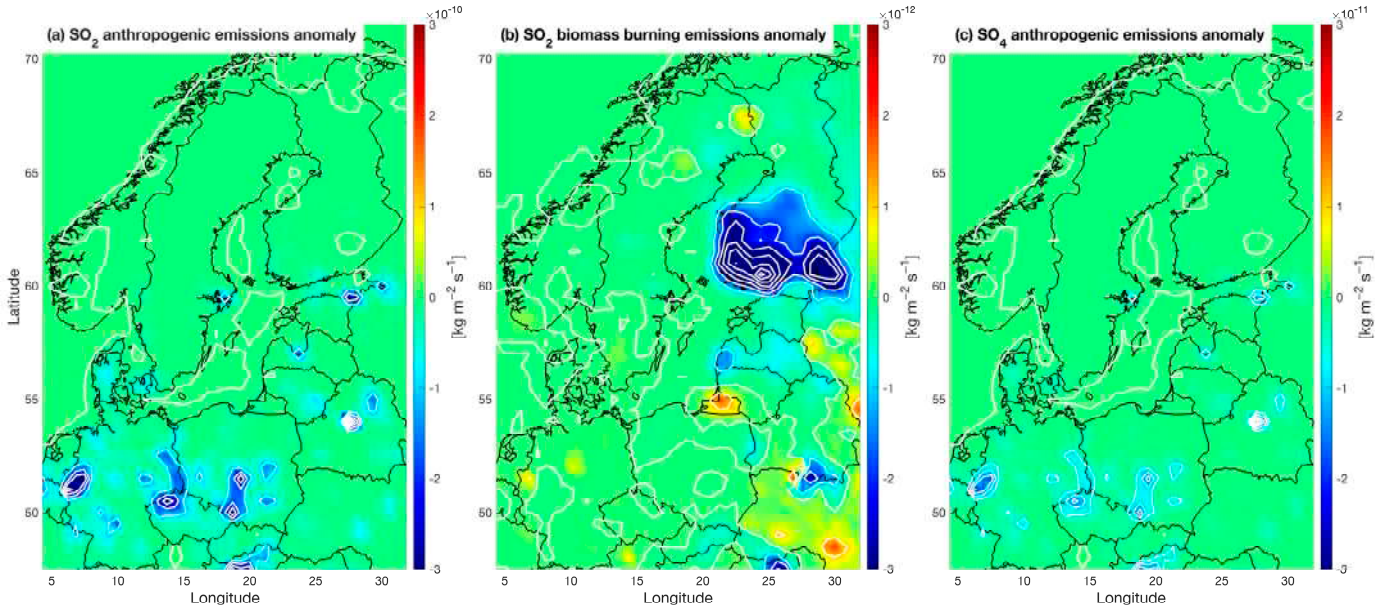

Figure 3. Spatial distribution of emissions anomalies between 2019 and 1989–2018 of (**a**) SO_2 from anthropogenic sources, (**b**) SO_2 from biomass burning, and (**c**) SO_4 from anthropogenic sources. Data drawn from the MERRA-2 emissions database for the study domain. Contour lines are in white colour.

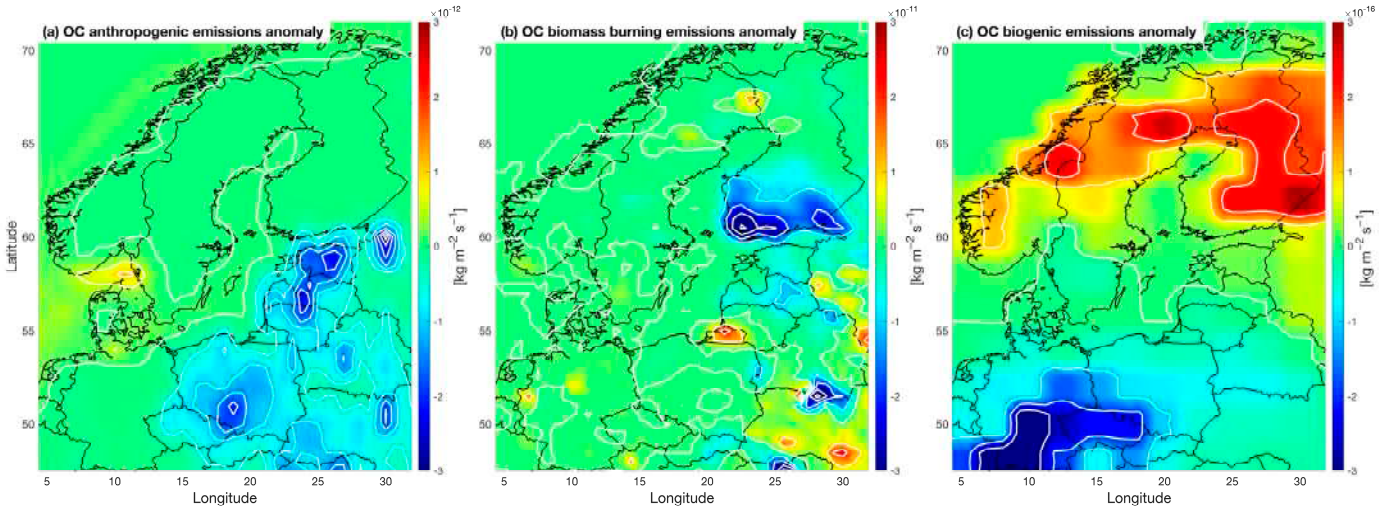

Figure 4. Spatial distribution of emissions anomalies of organic carbon (OC) between 2019 and 1989–2018 from (**a**) anthropogenic sources, (**b**) biomass burning, and (**c**) biogenic emissions. Data drawn from the MERRA-2 emissions database for the study domain. Contour lines are in white colour.

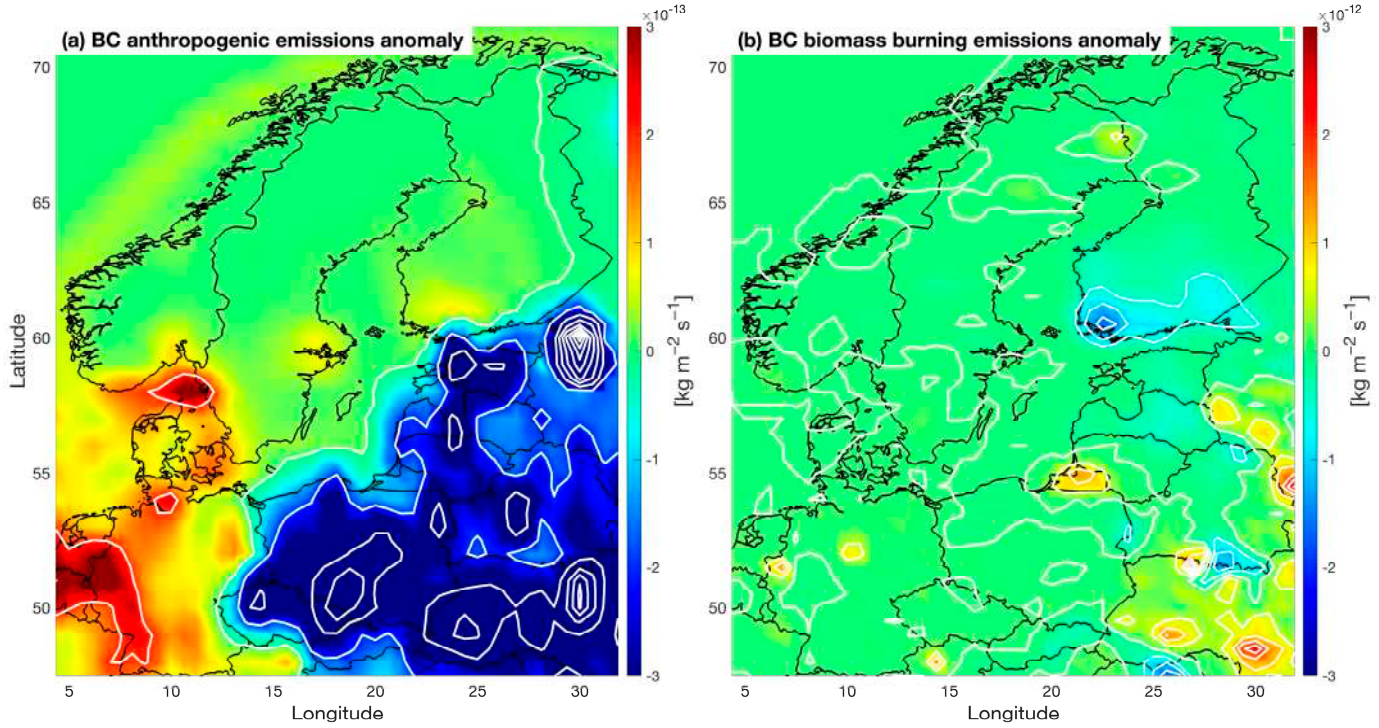

Figure 5. Spatial distribution of emissions of black carbon (BC) anomalies between 2019 and 1989–2018 from (**a**) anthropogenic sources, and (**b**) biomass burning. Data drawn from the MERRA-2 emissions database for the study domain. Contour lines are in white colour.

Anomalies of anthropogenic emissions of SO_2 and SO_4 (Figure 3a,c) were in relatively limited areas compared to the anomalies in SO_2 from biomass burning (Figure 3b). The highest anomalies in OC emissions originated in biomass burning, with up to 1 and 5 orders of magnitude higher values than the anomalies related to anthropogenic and biogenic emissions, respectively (Figure 4). Anomalies in BC emissions from biomass burning were about 1 order of magnitude larger than the anomalies in anthropogenic emissions of BC (Figure 5). According to Yang et al. [61], between 2010 and 2018 the average contribution of European emissions was 32–47% to the SO_4 AOD and 57–75% to the BC AOD levels over Europe.

Eastern Europe and the Baltic States showed negative anomalies in anthropogenic emissions of SO_2 (Figure 3a), SO_4 (Figure 3c), OC (Figure 4a), and BC (Figure 5a). Reductions in SO_X emissions from shipping occurred with the entry into force of MARPOL Annex VI, which set more stringent limits on the sulphur content of marine fuel in 2005 and 2015 in the Baltic Sea and North Sea (Figure A1). However, at the national level the contribution of shipping to total SO_X emissions was negligible compared to other emission sectors such as public power, industry, and other stationary combustion (Figures A1 and A2).

Negative anomalies in anthropogenic emissions of SO_2 (Figure 3a) and SO_4 (Figure 3c) appeared in Germany, Denmark, and Scandinavia, whereas anomalies in anthropogenic emissions were positive for OC and BC in Western Europe and a limited area between Denmark, Sweden, and Norway (Figures 4a and 5a). Anomalies in emissions of SO_2 (Figure 3b), OC (Figure 4b), and BC (Figure 5b) from biomass burning showed negative values in Southern Finland and the Baltic States. Positive biomass burning emissions anomalies appeared in Germany and Norway as hotspots, and as relatively large areas in non-European countries such as Ukraine and the Russian Federation.

3.2. Spatial Distribution of Mean Total and Main Aerosol Species AODs

Figure 6 maps the mean total and main aerosol species AODs in the study domain from 1989 to 2019. A gradient is clear for the maps of mean total and SO_4, BC, OC, and

dust AODs, with higher values at lower latitudes compared to higher latitudes in line with the findings by Saponaro et al. [62]. Mean total and SO_4 AODs hotspot areas were located around the regions in Poland (e.g., Silesia) and the Czech Republic (e.g., Moravia-Silesia) that have high-emitting industries. Filonchyk et al. [6] related the relatively high AOD values over Polish cities to the concentration of ferrous and non-ferrous, chemical, and mining industries. The mean OC AOD values were highest over the southeastern part of the domain (e.g., Ukraine and Belarus). Central and Western Europe showed the highest BC AOD levels (Figure 6d). The lowest mean total (Figure 6a), SO_4 (Figure 6b), OC (Figure 6c) and BC (Figure 6d) AOD levels were over the Scandinavian Mountains.

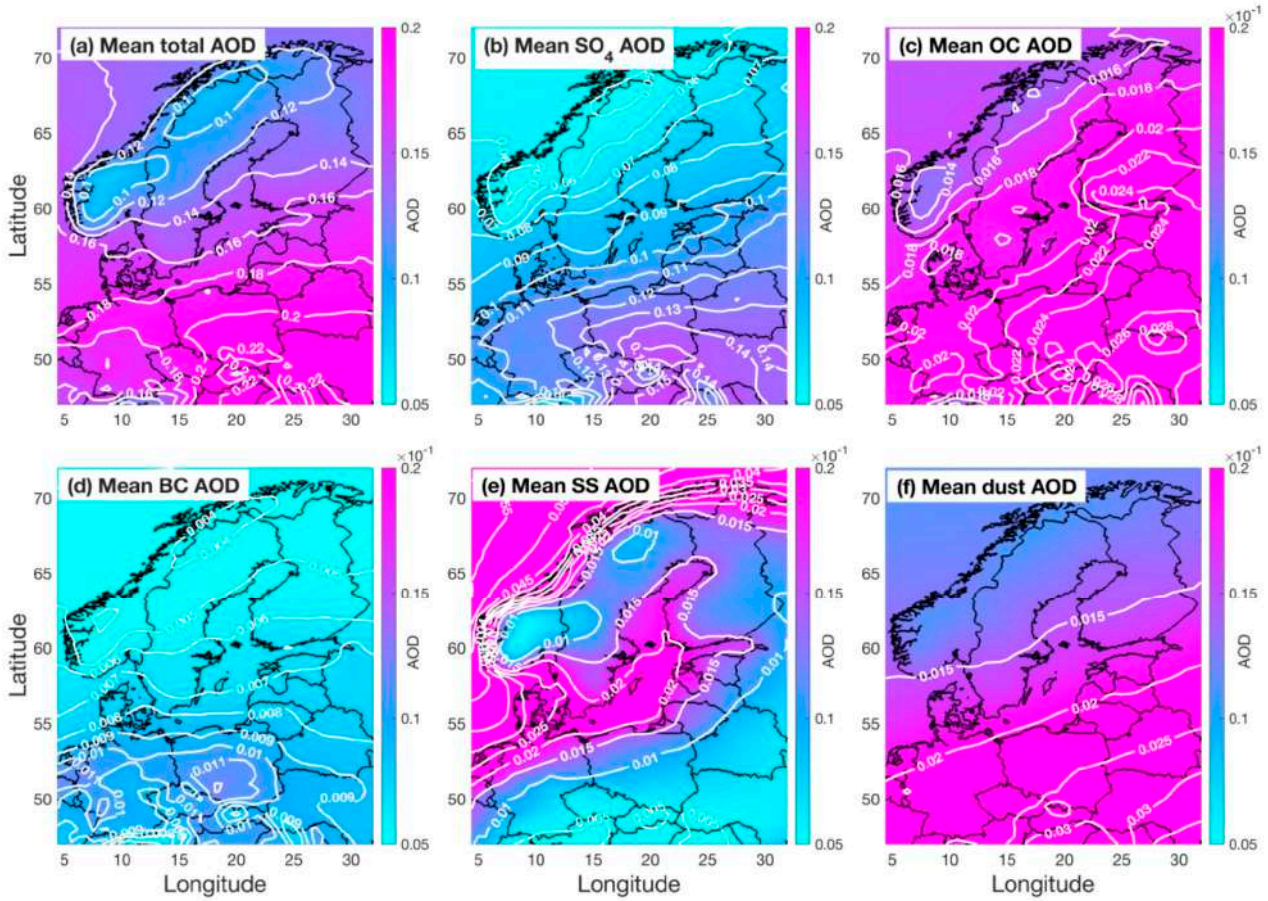

Figure 6. Spatial distribution of mean (**a**) total, SO_4 (**b**), OC (**c**), BC (**d**), SS (**e**), and dust (**f**) AODs in the study domain from 1989 to 2019 based on MERRA-2 reanalysis.

The spatial trend of mean dust AOD values likely reflected the distance from the Sahara Desert (i.e., the main source of desert dust for Europe) (Figure 6f). The highest values of mean SS AOD were above the Scandinavian peninsula because of more favourable conditions of SS formation compared to the relatively shallow and enclosed Baltic Sea (Figure 6e).

3.3. Yearly Mean AOD of Total Aerosol and the Main Aerosol Species

Figure 7 shows the yearly mean AOD trendlines of total and SO_4 AODs by MERRA-2 and the spaceborne aerosol observations derived from MODIS and MISR over the capitals of the Baltic Sea basin for the time range 1989–2019. The spaceborne aerosol observations are depicted in the dashed orange (MODIS) and purple (MISR) lines in the time ranges 2001–2019 and 2001–2017, respectively. Over each city, the MODIS AOD was generally higher than the MISR AOD. This is in line with the results reported by Zhao et al. [63] about AOD values retrieved with MISR and MODIS over different regions, including Western

Europe for a ten-year period (2007–2016). Mehta et al. [4] reported negative annual AOD trends over the European continent and the Mediterranean Sea from 2001 to 2014, with a higher decrease in total AOD for MODIS compared to MISR.

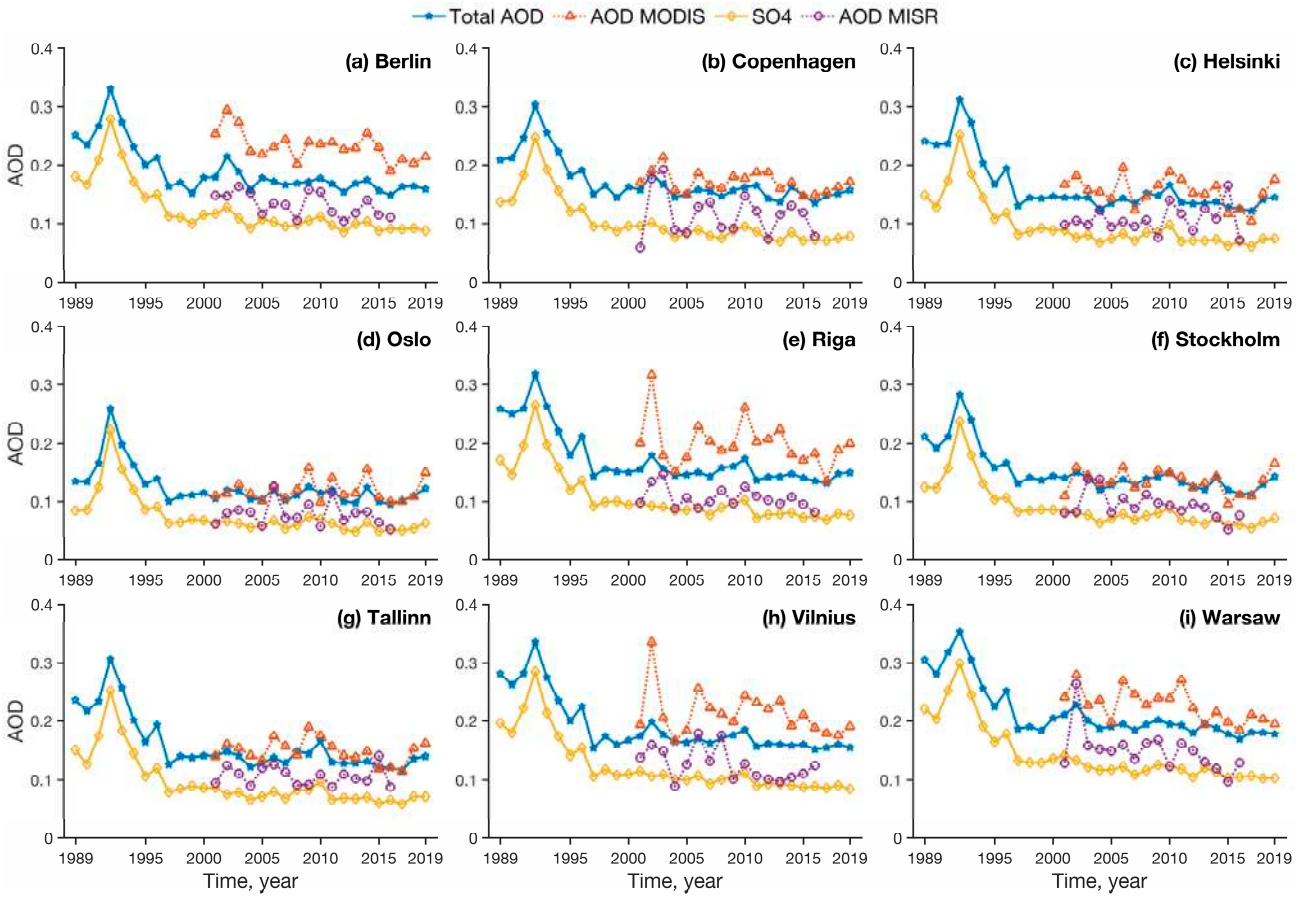

Figure 7. Yearly mean total and SO_4 aerosol optical depths (AODs) from MERRA-2 reanalysis, and total AOD derived from spaceborne MODIS and MISR observations over the capitals of countries in the Baltic Sea basin, namely (**a**) Berlin, (**b**) Copenhagen, (**c**) Helsinki, (**d**) Oslo, (**e**) Riga, (**f**) Stockholm, (**g**) Tallinn, (**h**) Vilnius, and (**i**) Warsaw from 1989 to 2019.

From 1989 to 2019, the MERRA-2 total and SO_4 AODs are shown in continuous lines. For each capital, the yearly mean SO_4 AOD (in yellow diamond markers) was the main aerosol species with a trend specular to yearly mean total AOD (in blue pentagram).

Analysing Figure 7, it may be noted that the MERRA-2 yearly mean total AOD values were in the range of 0.095–0.354, with the peak values associated with the Pinatubo eruption in 1991 [64,65].

A peak in the total and SO_4 AODs is clear for each capital in 1992. This was due to the dispersion of the volcanic plume that originated from the eruption of Mount Pinatubo (Philippines) in June 1991. Previous studies [2,66] reported the effects of the Mount Pinatubo eruption on the total and SO_4 AOD levels based on the MERRA-2 reanalysis around the world. Sun et al. [66] estimated an increase in total AOD over China for ten months followed by an 8-month-long decrease to AOD levels comparable to those measured before the eruption. Rizza et al. [2] reported variations in SO_4 AOD levels from July 1991 to December 1993 over five Italian cities. However, in MERRA-2 the representation of stratospheric aerosol produced from SO_2 oxidation after major volcanic eruptions may be biased by quality data of key eruption source parameters (i.e., plume height, injection magnitude, and mass eruption rate) [43,67]. After the eruption of Mount Pinatubo, MERRA-2 overestimated the total AOD and underestimated the AOD of non-sulphate aerosol species because the

same extinction coefficient was assumed for different sulphate aerosols irrespective of the size distribution [44].

For the selected cities, the mean MERRA-2 total AOD values were highest for the continental cities (Warsaw > Berlin > Vilnius) and the lowest for coastal cities such as Stockholm and Oslo (Table 2). The mean MERRA-2 total AOD values were comparably higher over coastal cities such as Copenhagen, Riga, Helsinki, and Tallinn.

Table 2. Descriptive statistics of total aerosol optical depth (AOD) and AOD of the main aerosol species over the capitals of countries in the Baltic Sea basin from 1989 to 2019.

City	Total AOD	SO_4 AOD	BC AOD	OC AOD	Dust AOD	SS AOD
Berlin	0.191 ± 0.043 (0.149–0.330)	0.124 ± 0.046 (0.085–0.280)	0.010 ± 0.001 (0.008–0.012)	0.021 ± 0.004 (0.013–0.030)	0.021 ± 0.005 (0.013–0.033)	0.014 ± 0.002 (0.011–0.018)
Copenhagen	0.174 ± 0.039 (0.135–0.303)	0.104 ± 0.042 (0.069–0.248)	0.008 ± 0.001 (0.006–0.010)	0.019 ± 0.004 (0.012–0.026)	0.018 ± 0.004 (0.011–0.026)	0.024 ± 0.003 (0.019–0.031)
Helsinki	0.164 ± 0.048 (0.121–0.312)	0.098 ± 0.043 (0.060–0.252)	0.007 ± 0.001 (0.005–0.010)	0.024 ± 0.011 (0.012–0.063)	0.017 ± 0.004 (0.010–0.024)	0.018 ± 0.002 (0.014–0.023)
Oslo	0.125 ± 0.034 (0.095–0.259)	0.076 ± 0.036 (0.049–0.222)	0.006 ± 0.001 (0.005–0.007)	0.018 ± 0.004 (0.011–0.026)	0.014 ± 0.003 (0.008–0.019)	0.011 ± 0.002 (0.008–0.014)
Riga	0.174 ± 0.048 (0.132–0.318)	0.109 ± 0.046 (0.069–0.264)	0.008 ± 0.001 (0.005–0.011)	0.023 ± 0.008 (0.012–0.058)	0.020 ± 0.004 (0.011–0.029)	0.015 ± 0.003 (0.010–0.020)
Stockholm	0.152 ± 0.039 (0.113–0.283)	0.092 ± 0.040 (0.054–0.236)	0.006 ± 0.001 (0.005–0.008)	0.019 ± 0.004 (0.012–0.027)	0.016 ± 0.003 (0.009–0.022)	0.019 ± 0.002 (0.014–0.022)
Tallinn	0.159 ± 0.047 (0.117–0.306)	0.096 ± 0.044 (0.059–0.252)	0.007 ± 0.001 (0.005–0.009)	0.022 ± 0.008 (0.012–0.049)	0.018 ± 0.004 (0.010–0.025)	0.016 ± 0.002 (0.012–0.020)
Vilnius	0.190 ± 0.049 (0.152–0.336)	0.125 ± 0.049 (0.084–0.285)	0.008 ± 0.001 (0.006–0.011)	0.024 ± 0.007 (0.013–0.044)	0.023 ± 0.005 (0.013–0.032)	0.010 ± 0.002 (0.007–0.014)
Warsaw	0.216 ± 0.049 (0.169–0.354)	0.145 ± 0.051 (0.103–0.299)	0.011 ± 0.001 (0.008–0.014)	0.026 ± 0.005 (0.016–0.037)	0.025 ± 0.006 (0.014–0.037)	0.009 ± 0.001 (0.006–0.011)

Annual mean BC AODs were in the range of 0.005–0.014 (black colour at the bottom of each panel in Figure 8). Except for Warsaw, the mean BC AOD was the aerosol species with the lowest level (Table 2) for the time range considered. OC AODs (orange colour in Figure 8) ranged between 0.11 and 0.063. Natural aerosols species showed a similar trend, with dust (yellow hexagram markers) and SS (blue triangle marker) AODs values between 0.006 and 0.037.

The order of magnitude of the mean OC, DU, and SS AOD species differed for the selected cities (Table 2). Mean SS AODs were lower than mean OC, and DU AODs both for the continental cities and the coastal cities such as Oslo, Riga, and Tallinn. Over the continental cities, the mean OC AODs were comparable to mean DU AODs, whereas mean OC AODs were higher than mean DU AODs over Oslo, Riga, and Tallinn. The mean DU AODs were lower than the mean SS and OC AODs over coastal cities such as Copenhagen, Helsinki, and Stockholm. These cities differed in the magnitude of the mean OC and SS AOD species, with the mean OC AODs higher or comparable to the mean SS AODs over Helsinki and Stockholm, respectively, and the mean SS AOD higher than the mean OC AOD over Copenhagen.

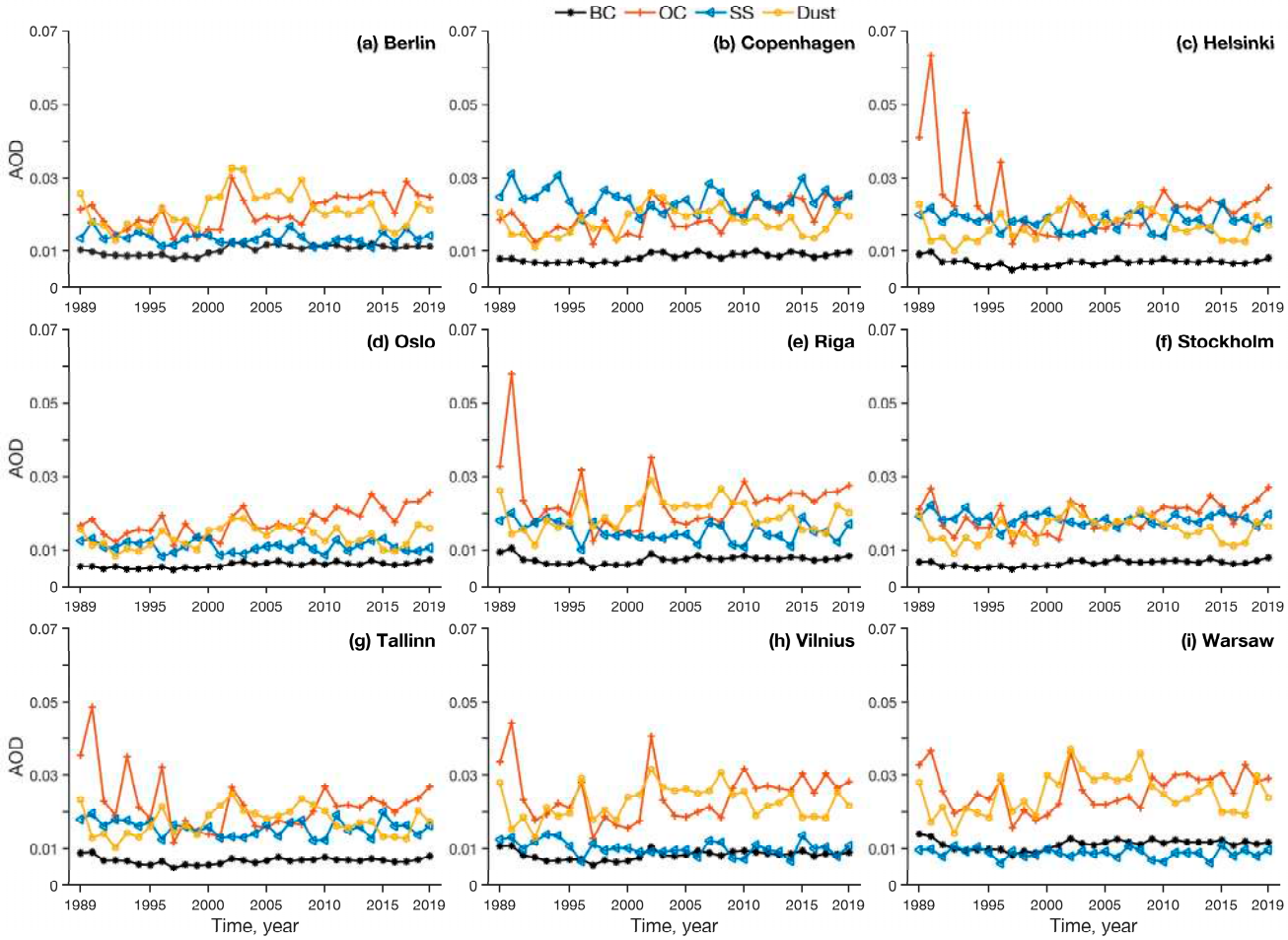

Figure 8. Yearly mean aerosol optical depth (AOD) of black carbon (BC), organic carbon (OC), sea salt (SS), and dust from MERRA-2 reanalysis over the capitals of countries in the Baltic Sea basin, namely (**a**) Berlin, (**b**) Copenhagen, (**c**) Helsinki, (**d**) Oslo, (**e**) Riga, (**f**) Stockholm, (**g**) Tallinn, (**h**) Vilnius, and (**i**) Warsaw from 1989 to 2019.

3.4. Percentage Contributions of the Main Aerosol Species to Total AOD

In each capital, the percentage contribution of the SO_4 AOD to the total AOD peaked in 1992, the year following the eruption of Mount Pinatubo, with values in the range of 80.1–85.8% of the total AOD (Figure 9). Table 3 reports the mean and range of contribution in the percentage of the main aerosol species to the total AOD for each capital.

Our analysis of the percentage contributions of the main aerosol species to the total AOD over Warsaw is comparable to Markowicz et al. [68], who reported the mean AOD composition over Poland to be dominated by the SO_4 AOD (70%), followed by the OC and DU AODs (10% each), BC AOD (5%), and SS AOD (4%) between 1982 and 2015, based on MERRA-2 reanalysis.

We conclude that for all of the capitals, the composition of aerosols changed with respect to the species of anthropogenic origins, with a decrease in the percentage contribution of the SO_4 AOD and an increase in the percentage contribution of the BC AOD to the total AOD. For Copenhagen, Oslo, Stockholm, and the continental capitals, the OC AOD percentage also showed an increasing trend. Variations in the composition of the AOD over Europe were also observed in previous studies [3,11] for the first two decades of the 21st century.

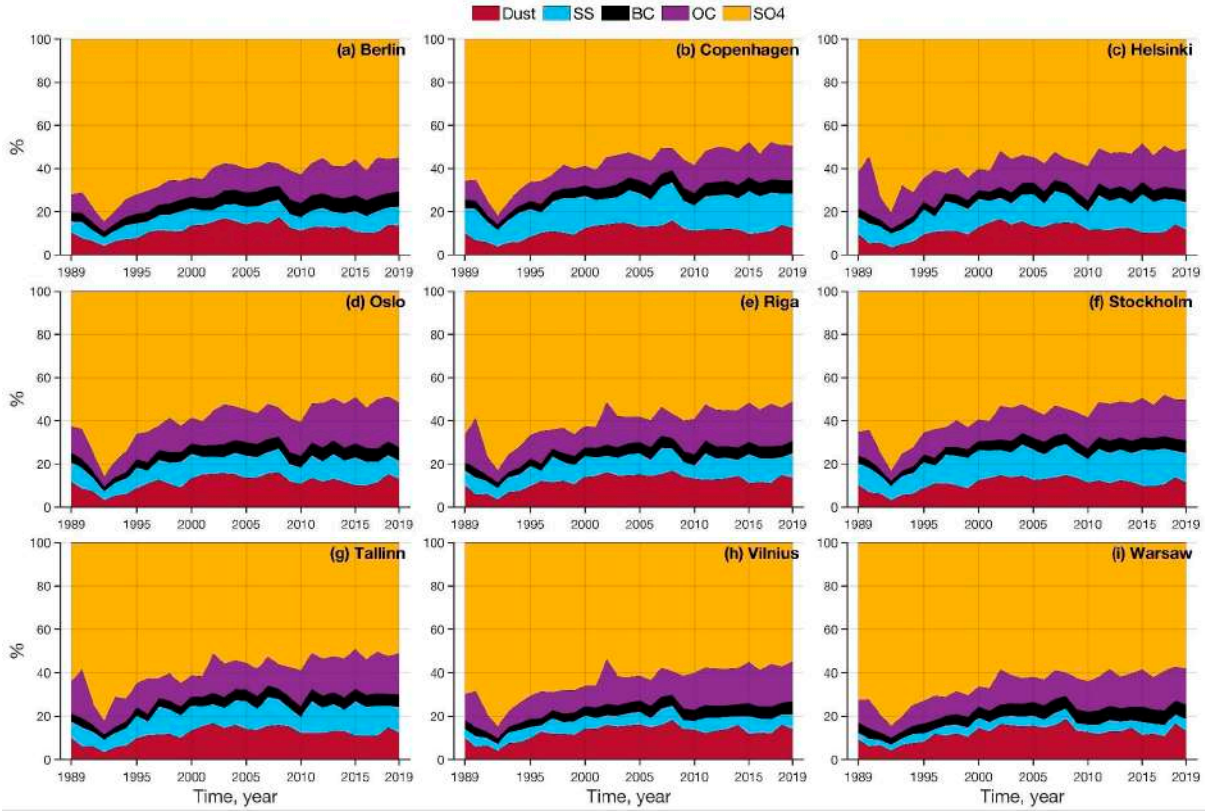

Figure 9. Percentage contributions of the main aerosol species to total aerosol optical depth over the capitals of countries in the Baltic Sea basin, namely (**a**) Berlin, (**b**) Copenhagen, (**c**) Helsinki, (**d**) Oslo, (**e**) Riga, (**f**) Stockholm, (**g**) Tallinn, (**h**) Vilnius, and (**i**) Warsaw from 1989 to 2019. BC—black carbon; OC—organic carbon; SS—sea salt.

Table 3. Contributions in percentage of the main aerosol species to total aerosol optical depth over the capitals of countries in the Baltic Sea basin from 1989 to 2019.

City	SO_4 [%]	BC [%]	OC [%]	Dust [%]	SS [%]
Berlin	63.8 (55.0–84.8)	5.7 (2.7–7.2)	11.5 (4.4–17.8)	11.7 (3.9–17.5)	7.4 (4.2–10.1)
Copenhagen	58.2 (47.5–81.9)	5.0 (2.3–6.3)	11.6 (4.1–17.3)	10.9 (3.6–15.8)	14.3 (8.1–20.3)
Helsinki	58.1 (48.4–80.7)	4.5 (2.3–5.6)	14.5 (7.1–26.8)	11.2 (3.2–16.5)	11.7 (6.6–18.1)
Oslo	59.1 (48.8–85.8)	5.0 (2.1–6.4)	15.0 (4.7–22.7)	11.6 (3.3–16.2)	9.2 (4.1–13.1)
Riga	60.6 (51.0–83.1)	4.5 (2.3–5.7)	13.8 (5.6–23.2)	12.1 (3.5–16.9)	9.0 (4.8–13.5)
Stockholm	58.7 (48.0–83.5)	4.5 (2.1–5.7)	13.2 (4.7–19.0)	10.9 (3.2–15.0)	12.7 (6.5–17.0)
Tallinn	58.9 (48.9–82.3)	4.5 (2.3–5.8)	14.3 (6.2–22.4)	11.8 (3.4–16.8)	10.5 (5.9–16.3)
Vilnius	64.0 (53.7–84.9)	4.6 (2.3–5.9)	13.3 (5.3–20.5)	12.6 (3.9–18.1)	5.5 (2.9–8.5)
Warsaw	65.8 (57.1–84.6)	5.4 (2.8–6.9)	12.4 (5.6–18.1)	12.1 (4.0–18.6)	4.2 (2.4–6.1)

Values are shown as mean (minimum–maximum).

3.5. Percentage Contributions of the Main Aerosol Species of Anthropogenic and Natural Origins to Total AOD

Figure 10 shows the time series of the percentage contributions of the main aerosol species of anthropogenic (i.e., SO_4 + BC + OC) and natural (i.e., DU + SS) origins to the total AOD over the capitals of the study area.

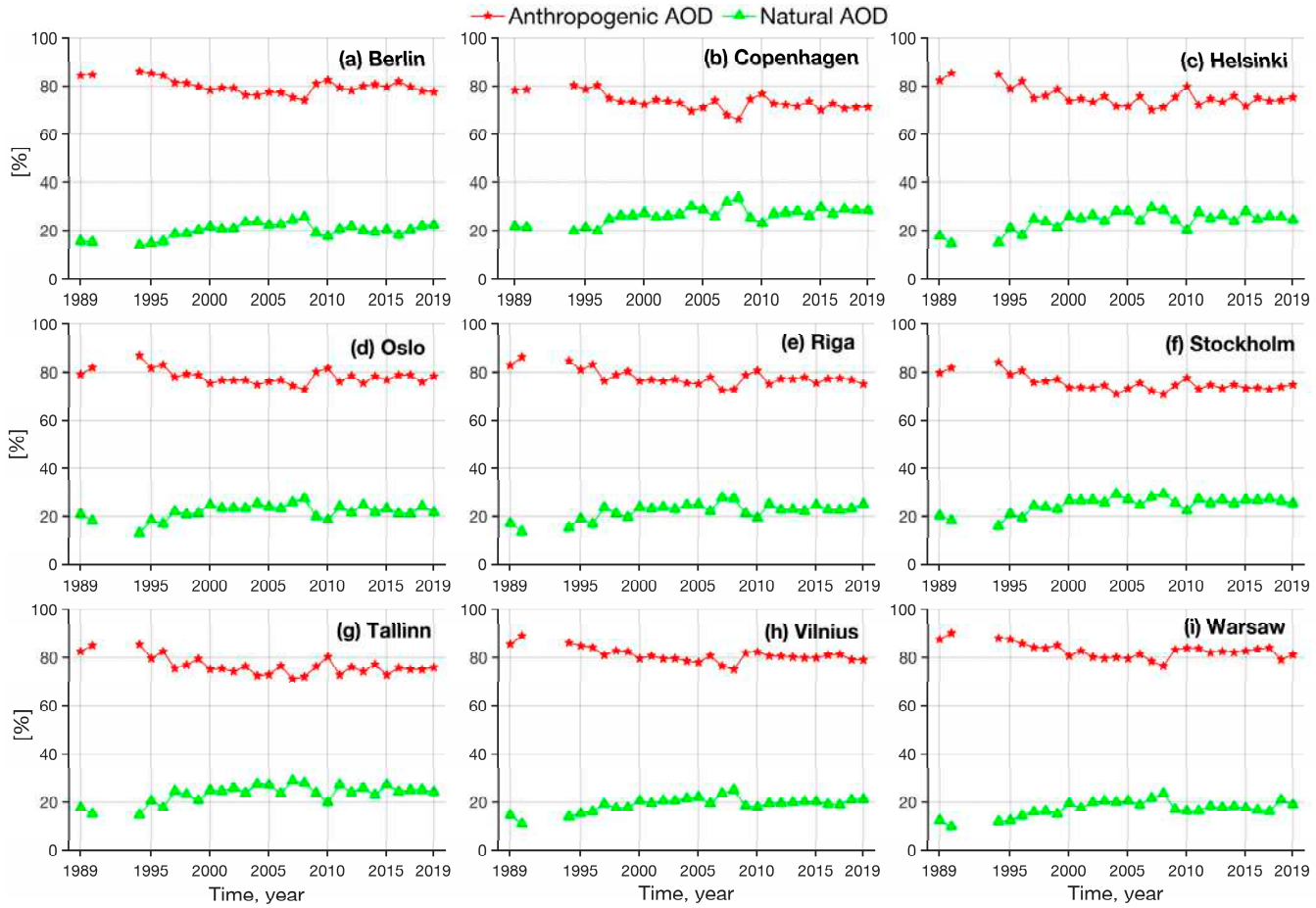

Figure 10. Percentage contributions of the main aerosol species of anthropogenic (i.e., sulphate, black carbon, and organic carbon) and natural (i.e., dust and sea salt) origins to total aerosol optical depth (AOD) for the capitals of countries in the Baltic Sea basin, namely (**a**) Berlin, (**b**) Copenhagen, (**c**) Helsinki, (**d**) Oslo, (**e**) Riga, (**f**) Stockholm, (**g**) Tallinn, (**h**) Vilnius, and (**i**) Warsaw from 1989 to 2019. Data gap between 1991 and 1993 is due to the perturbation in the distribution of the main aerosol species following the eruption of Mount Pinatubo.

Anthropogenic aerosols contributed the most to the total AOD over all the capitals, with percentages in the range of 66.4–90.3%. The highest values in the percentage of anthropogenic AOD were over the continental capitals, whereas the lowest value in the percentage of anthropogenic AOD was over Copenhagen.

Previous studies [5,6] reported the predominance of fine particles of anthropogenic origins in AOD over Eastern countries including Poland between 2000–2019. According to Zhao et al. [63], particles of anthropogenic origins (polluted continental/dust) are the dominant aerosol type above Western Europe, including Denmark, Germany, and a limited portion of Norway and Sweden based on analysis of data drawn from CALIPSO retrievals from 2007 to 2016.

The minimum in the percentage contribution of anthropogenic AOD appeared in 2008 for all capitals except Helsinki and Tallinn, with the minimum in 2007. This was likely due

to the global financial crisis in 2008 and the so-called Great Recession from December 2007 to June 2009.

Together with the economic crisis of 2008–2009, variations in the aerosol composition over Vilnius likely resulted from changes in the energy sector following the shutdown of the Ignalina nuclear power plant in Lithuania in 2009. Between 2009 and 2019, carbon intensity consistently increased in Lithuania (Figure 2d).

3.6. Annual Trends

3.6.1. Annual Trends in MERRA-2 Anthropogenic Emissions of SO_2, Black Carbon, and Organic Carbon

We estimated the yearly trends in anthropogenic emissions of SO_2, BC, and OC from the capitals of the Baltic Sea basin based on the MERRA-2 database in the time range 1989–2019 (Figures 11 and 12).

Anthropogenic emissions of SO_2 significantly decreased in each capital, with all of the capitals except Oslo in the range of -0.01 and -0.03 [kg m^{-2} s^{-1} year^{-1}], 0.54–0.89 $R^{2,}$ and *p*-values far below 0.0001 (Table A2). Anthropogenic emissions of BC and OC showed a significant decreasing trend in each capital except Copenhagen. The highest decreases in anthropogenic BC and OC emissions were in Helsinki, the capitals of the Baltic states, and Warsaw, with R^2s in the range of 0.19–0.53, *p*-values below 0.01, and rates of decrease between -0.01 and -0.02 [kg m^{-2} s^{-1} year^{-1}] (Table A2). According to Yang et al. [61], SO_2 and BC emissions decreased by 84–93% and 43–62% in 2014–2018 compared with 1980–1984 in northwestern and eastern Europe.

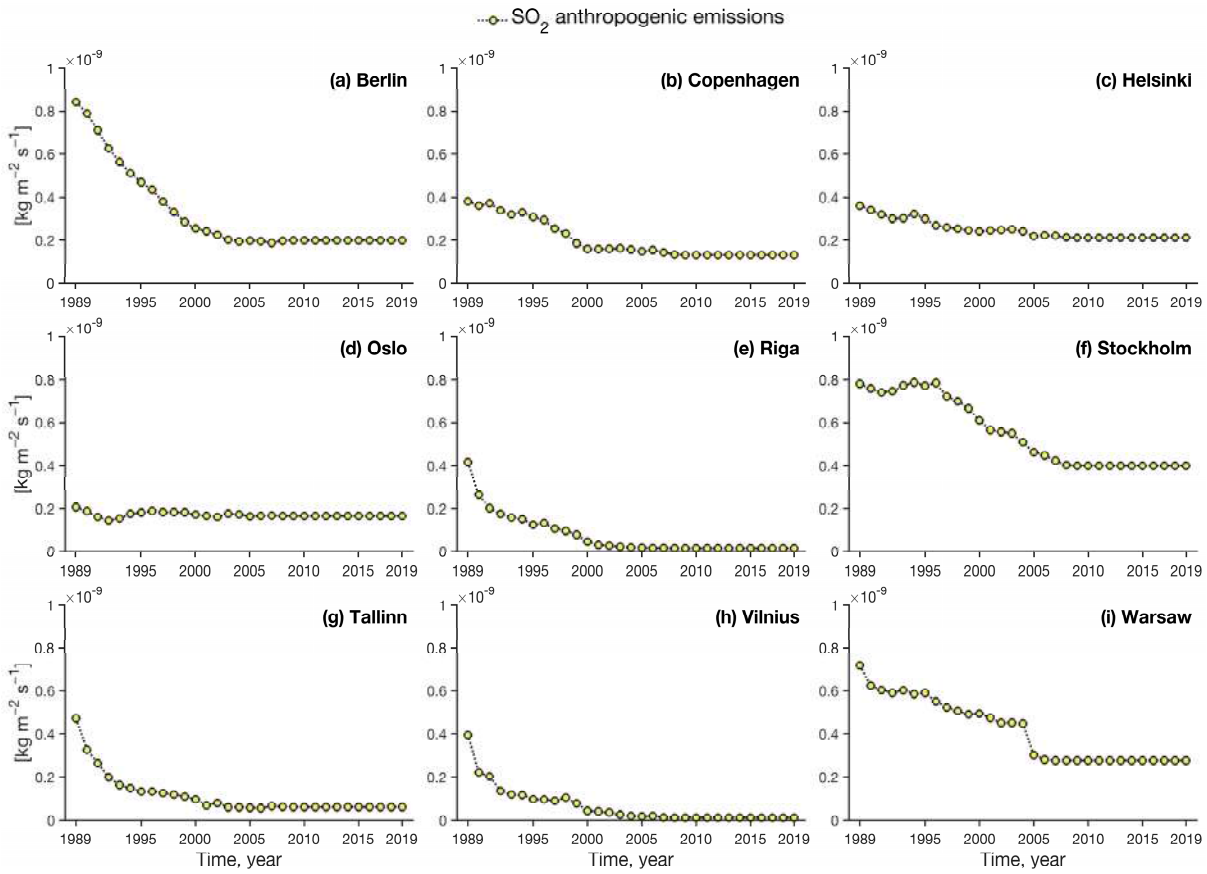

Figure 11. MERRA-2 anthropogenic emissions from the capitals of countries in the Baltic Sea basin, namely (**a**) Berlin, (**b**) Copenhagen, (**c**) Helsinki, (**d**) Oslo, (**e**) Riga, (**f**) Stockholm, (**g**) Tallinn, (**h**) Vilnius, and (**i**) Warsaw from 1989 to 2019.

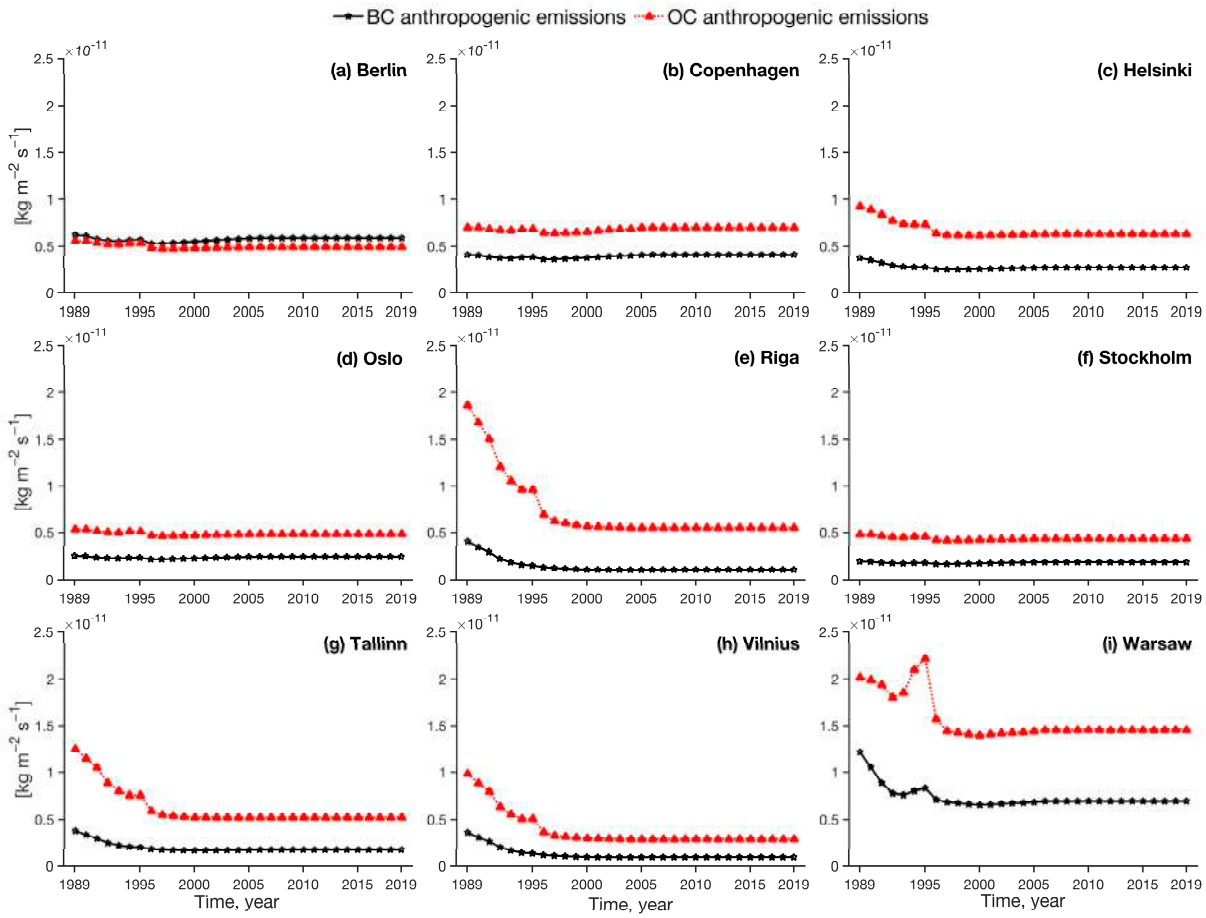

Figure 12. MERRA-2 anthropogenic emissions of black carbon (BC) and organic carbon (OC) from the capitals of countries in the Baltic Sea basin, namely (**a**) Berlin, (**b**) Copenhagen, (**c**) Helsinki, (**d**) Oslo, (**e**) Riga, (**f**) Stockholm, (**g**) Tallinn, (**h**) Vilnius, and (**i**) Warsaw from 1989 to 2019.

Variations in anthropogenic emissions of BC, OC (Figure 12), and SO_2 (Figure 11) mainly occurred between 1989 and 2005. No substantial changes in anthropogenic emissions occurred between 2005 and 2019. In the 1990s, all of the capitals except Oslo and Stockholm showed sharp decreases in anthropogenic emissions of SO_2 (Figure 11). Moreover, in the 1990s sharp decreases in anthropogenic emissions of BC and OC occurred in Helsinki, the capitals of the Baltic states, and Warsaw (Figure 12).

3.6.2. Annual Trends in the Main Aerosol Species and Total AODs

From 1989 to 2019, the MERRA-2 total and SO_4 AODs showed a significant decreasing trend for all the capitals (Table A3).

For the decreasing trends in total AOD, values of R^2 were in the range of 0.29–0.6, *p*-values below 0.003, and rates of decrease between −0.3 and −1.6% year^{-1} (Table A3). The decreasing trends in SO_4 AOD showed *p*-values far below 0.00001, R^2 in the range 0.49–0.73, and rates of variation between −0.9 and −2% year^{-1}. Cities with the highest mean yearly total and SO_4 AODs (Table 2), such as Warsaw and Vilnius, showed the highest rate of yearly decrease in total and SO_4 AODs (Table A3). Oslo was the city with the lowest mean yearly total and SO_4 AODs (Table 2) and the lowest rate of yearly decrease in total and SO_4 AODs (Table A3). This means that the decrease in total AOD was mainly due to a decrease in SO_4 AOD.

By contrast, both the OC and BC AODs significantly increased over Berlin, Copenhagen, and Oslo, with BC AOD an order of magnitude lower compared with the OC AOD. Moreover, the BC AOD significantly increased over Stockholm. Provençal et al. [1] observed that the SO_4, OC, and BC AOD trends are likely to be similar, because fossil

fuel combustion is a major source of these anthropogenic AOD species. Therefore, it is likely that the increasing trends in OC and BC AODs for Berlin, Copenhagen, Oslo, and Stockholm were due to biomass combustion for heating purposes or because of wildfires. Smoke plumes over Eastern, Western, and Northern Europe often originate from forest and peat fires or agricultural and pastoral burning in Russia and Ukraine in spring, summer, and autumn [5].

It is important to point out that the observed decreases in the total and SO_4 AODs mainly occurred in the 1990s over the selected capitals. Figure A2 shows a sharp decrease in total SO_X emissions for the countries in the Baltic Sea basin. Yang et al. [61] related the lower SO_4 AOD levels between 1980–1984 and 2014–2018 in Europe to decreases in local European sources for about 89% of the differences, and only 9% and 7% to decreases in emissions from the Russian Federation-Belarus-Ukraine and North America, respectively. For the time range 2000–2021, our results align with Di Antonio et al. [7] who did not observe any statistical trends for the AOD from MAIAC over Copenhagen, Oslo, and Stockholm. For these cities, this is clearly shown by comparing the time series of the total and SO_4 AODs between the time ranges of 1989–1999 and 2000–2019 (Figure 7b,d,f). Markowicz et al. [68] reported a negative trend for total the AOD over different regions of Poland including Warsaw (−0.06 per decade) between 1982 and 2015, with the AOD composition showing a similar negative trend in the SO_4 AOD, and a small positive trend in OC. In Poland, in the 1991–2000 decade the reduction in industrial emissions likely led to a strong decrease (−0.17/10 year) in AOD levels [68], whereas a shift of the energy mix to green fuel for residential heating likely originated a slight decrease (−0.02/10 year) in the AOD levels from 2011 to 2019 [14].

3.6.3. Annual Trends in the Percentage Contributions of the Main Aerosol Species to the Total AOD

We evaluated the trend in the percentage contributions of the main aerosol species to the total AOD, excluding the time range 1991–1993 because of the perturbation in the percentage distribution of AOD species occurring with the dispersion and deposition of SO_4 related to the Mount Pinatubo eruption (Table A4).

In this time range, all of the capitals showed a significant decreasing trend in the percentage contribution of the SO_4 AOD to the total AOD, with R^2 values in the range of 0.53–0.78 and *p*-values far below 0.001. By contrast, the percentage contribution of the BC AOD to the total AOD significantly increased over all the capitals, with R^2 values in the range of 0.73–0.85 and *p*-values far below 0.001.

The capitals differed in the trend of the percentage contribution of the OC AOD to the total AOD, with some capitals showing no trend (i.e., Helsinki) or a slight increasing trend (i.e., Riga, and Tallinn with R^2 up to 0.20 and *p*-value equal to 0.201 and 0.168, respectively), and the other capitals showing significant increasing trends with R^2 values in the range of 0.42–0.76 and *p*-values < 0.001.

The percentage contribution of aerosol components of natural origins to the total AOD did not show any remarkable trend over the capitals, except for an increasing trend in the percentage contribution of the SS AOD to the total AOD over Helsinki and Stockholm. Specifically, the percentage contribution of the SS AOD to the total AOD showed no trend over Oslo and Vilnius, a slight increasing trend over Berlin, Copenhagen, Warsaw, and Riga (R^2 values < 0.25 and *p*-values up to 0.03), and an increasing trend over Helsinki and Stockholm with an R^2 equal to 0.30 and 0.39, respectively, and *p*-values < 0.001. The percentage contribution of the dust AOD to the total AOD showed no trend over Berlin, Oslo, and Stockholm and a slight increasing trend over the other capitals with R^2 value up to 0.28 and *p*-values < 0.05. The work by Logothetis et al. [69] analysed the MODIS dust aerosol fine-resolution dataset and found a slight decreasing trend for the dust optical depth over the Mediterranean area between 2003 and 2017.

3.6.4. Annual Trends in the Percentage Contributions of Anthropogenic and Natural AOD to the Total AOD

From 1989 to 2008, anthropogenic AOD as a percentage of the total AOD showed a significant decreasing trend for all the capitals, with R^2 in the range 0.6–0.88, *p*-values far below 0.0001, and rate of yearly decrease between −0.4 and −0.7 (Table A5). The percentage contribution of natural aerosols to the total AOD showed a reverse trend in each city, with R^2 in the range of 0.6–0.88, *p*-values far below 0.0001, and a yearly increase rate between 0.4 and 0.7.

According to Naqvi [15], European regions experienced a decoupling of economic growth and emissions of NH_3, NO_X, PM_{10}, $PM_{2.5}$, and SO_2 between 1995 and 2008, whereas several EU regions showed a coupling or a slight decoupling from 2008 to 2015.

3.6.5. Annual Trends in the Total and SO_4 AOD Described with Predictive Variables

Based on the stepwise linear regression method, we evaluated a set of independent variables (i.e., annual data of GDP per capita, energy efficiency, and SFFGAE) in describing the total and SO_4 AOD levels over the capitals from 2000 to 2019.

Annual data of SFFGAE and time were predictive variables for both the total and SO_4 AODs, whereas annual data of GDP per capita were predictive variables only for the SO_4 AOD. No relationships were found between the annual data of energy efficiency at the national level and the total and SO_4 AOD values over each capital.

Figure 13 shows the total and SO_4 AODs plotted versus the significant ($p < 0.05$) predictive variables for Helsinki, Oslo, Stockholm, Tallinn, and Vilnius from 2000 to 2019.

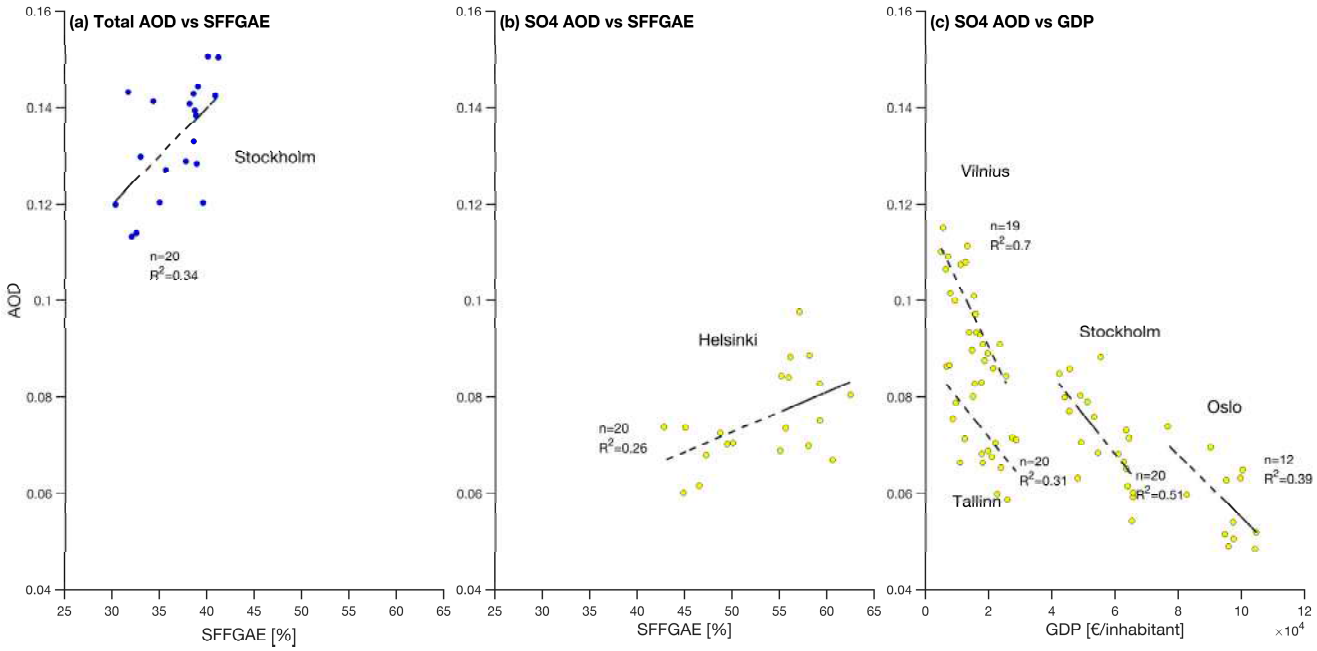

Figure 13. Total and SO_4 AODs plotted versus their respective predictive variables, namely (**a**,**b**) share of fossil fuel in gross available energy (SFFGAE), and (**c**) gross domestic product (GDP) per capita for Helsinki, Oslo, Stockholm, Tallinn, and Vilnius from 2000 to 2019. $p < 0.05$.

There were direct relationships between SFFGAE in Sweden and the total AOD over Stockholm (Figure 13a). Therefore, the higher the annual values of SFFGAE, the higher the total AOD levels over Stockholm.

The SO_4 AOD over Helsinki can be represented with a linear equation with the SFFGAE of Finland (Figure 13b). Therefore, the higher the annual values of SFFGAE, the higher the SO_4 AOD levels over Helsinki.

GDP per capita was the predictive variable of the SO_4 AOD over Oslo, Stockholm, Tallinn, and Vilnius, with inverse relationships and R^2s in the range 0.31–0.70 (Figure 13c).

Therefore, the higher the annual values of GDP per capita, the lower the SO_4 AOD levels over Oslo, Stockholm, Tallinn, and Vilnius.

The total and SO_4 AOD confirmed a decreasing linear trend with time for Berlin and Warsaw (Table A6), as presented in Paragraph 3.6.2. For Copenhagen, there was no relationship between the total and SO_4 AODs and the set of independent variables.

4. Conclusions

This study analysed the trends of total aerosol and the main aerosol species over the capitals of nine countries in the Baltic Sea basin from 1989 to 2019 based on the Modern-Era Retrospective Analysis for Research and Applications, Version 2 reanalysis. Aerosol speciation includes both natural [mineral dust (DU) and sea salt (SS)] and anthropogenic [sulphate (SO_4), organic carbon (OC), and black carbon (BC)] aerosols.

The mean total AOD values were the highest over the continental capitals (i.e., Warsaw, Berlin, and Vilnius), with values in the range 0.190–0.216, followed by the coastal capitals, namely Copenhagen, Riga, and Helsinki (0.164 and 0.174), and Tallinn, Stockholm, and Oslo (0.125–0.159).

For each capital, the mean SO_4 AOD was the main aerosol species, following a trend specular to total AOD. Apart from Warsaw, the mean BC AOD was the aerosol species with the lowest level. The orders of magnitude of mean OC, DU, and SS AODs differed across the capitals.

Over all the capitals, the composition of the aerosols changed with respect to the species of anthropogenic origins, with the percentage contributions to the total AOD decreasing for the SO_4 AODs and increasing for the BC AODs. For Copenhagen, Oslo, Stockholm, and the continental capitals, the OC AOD also showed an increase in its percentage contribution to the total AOD.

Anthropogenic aerosols contributed the most to the total AOD over all the capitals, with percentages in the range 66.4–90.3%. The highest values in the percentage of anthropogenic AODs were over the continental capitals, whereas the lowest value in the percentage of anthropogenic AOD was over Copenhagen. For all of the capitals, the minimum in the percentage contribution of anthropogenic AOD was between 2007 and 2008, likely due to the global financial crisis. Moreover, from 1989 to 2008, anthropogenic AOD as a percentage of the total AOD showed a significant decreasing trend.

From 1989 to 2019, the total and SO_4 AODs showed a significant decreasing trend for all of the capitals. Warsaw and Vilnius showed the highest rates of yearly decrease in the total and SO_4 AODs, whereas Oslo was the city with the lowest yearly decrease in the total and SO_4 AODs. Both the OC and BC AODs significantly increased over Berlin, Copenhagen, and Oslo. Moreover, the BC AOD significantly increased over Stockholm. Analysis of the MERRA-2 anthropogenic emissions database showed significant decreases in SO_2 from each capital and BC and OC in each capital except Copenhagen. Therefore, the observed increases in the OC and BC AODs did not result from variations in anthropogenic emissions from Berlin, Copenhagen, Stockholm, and Oslo. The decoupling of carbonaceous aerosols and the SO_4 AOD trends was likely due to concurrent factors such as low-sulphur fuel policies and biomass burning in wildfires or for energy production.

To account for the drastic changes in the demographic and economic perspectives that the study area experienced, we considered energy statistics and gross domestic product (GDP) per capita as potential predictors of the anthropogenic AOD components in the atmosphere over each city. In the first two decades of the 21st century, there were direct relationships between SFFGAE in Sweden and the total AOD over Stockholm. Moreover, there were direct relationships between SFFGAE in Finland and the SO_4 AOD over Helsinki. On the other hand, there were inverse relationships between the annual values of GDP per capita and the SO_4 AOD for Oslo, Stockholm, Tallinn, and Vilnius. Therefore, a relative decoupling between economic growth and the emissions of aerosols from fossil fuel may have occurred for these capitals.

As for caveats and uncertainties associated with this study, it is important to point out that atmospheric aerosol comprises a complex mixture of primary and secondary species whose interactions with chemistry, radiation, land use, and atmospheric circulation patterns cannot be addressed with the methods of the present study. These rather may be the objective of a future specific study utilizing a high (spatial/temporal) resolution chemical transport model.

Author Contributions: Conceptualisation, E.M. and U.R.; methodology, E.M.; validation, E.M.; formal analysis, E.M.; investigation, E.M.; resources, G.P.; data curation, E.M.; writing—original draft preparation, E.M.; writing—review and editing, E.M. and U.R.; visualization, E.M. and S.V.; supervision, G.P. and U.R.; project administration, G.P. and U.R. All authors have read and agreed to the published version of the manuscript.

Funding: This research received no external funding.

Data Availability Statement: The aerosol data set presented in this study is freely available in GIOVANNI (Goddard Earth Sciences Data and Information Services Center Interactive Online Visualization ANd aNalysis Infrastructure) at https://giovanni.gsfc.nasa.gov/giovanni/. The population [demo_r_pjanaggr3__custom_8310012], gross domestic product [NAMA_10R_3GDP__custom_8309870], energy efficiency [nrg_ind_eff__custom_8310117], and share of fossil fuels in gross available energy [nrg_ind_ffgae__custom_8310088] data are freely available in EUROSTAT at https://ec.europa.eu/eurostat.

Acknowledgments: The authors acknowledge the NASA GES-DISC Interactive Online Visualization and Analysis Infrastructure (GIOVANNI) for providing MERRA-2 reanalysis, MODIS, and MISR satellite aerosol data.

Conflicts of Interest: The authors declare no conflicts of interest.

Appendix A

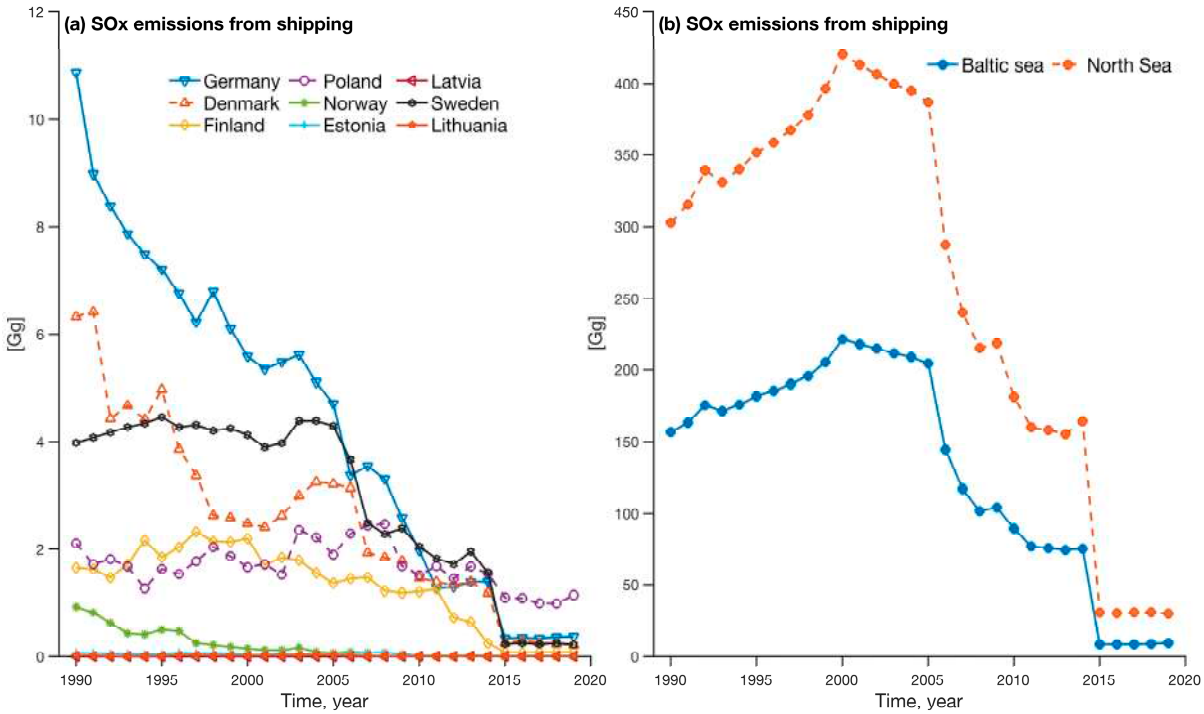

Figure A1. SO_X emissions from shipping from the (**a**) investigated countries in the Baltic Sea basin and (**b**) the Baltic Sea and North Sea. Own elaboration based on data from EMEP (https://www.ceip.at/webdab-emission-database/emissions-as-used-in-emep-models, accessed on 6 June 2024).

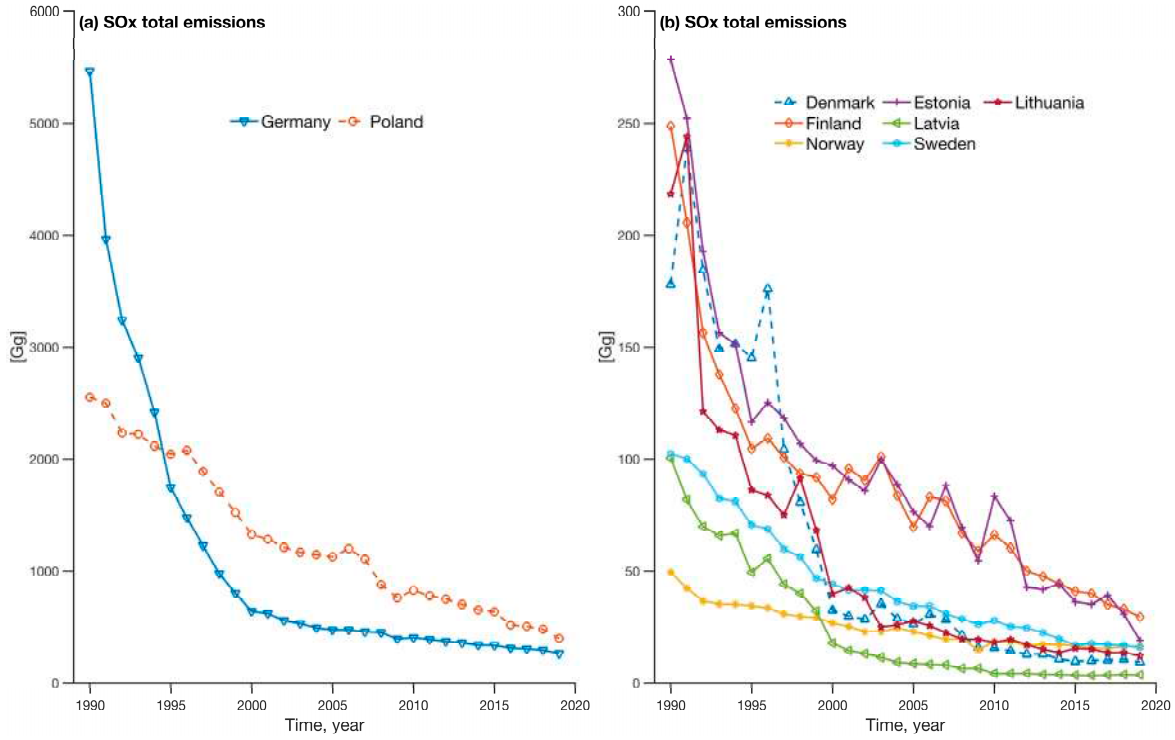

Figure A2. Total SO_X emissions from (**a**) Germany and Poland and (**b**) Denmark, Estonia, Finland, Latvia, Lithuania, Norway, and Sweden. Own elaboration based on data from EMEP (https://www.ceip.at/webdab-emission-database/emissions-as-used-in-emep-models, accessed on 6 June 2024).

Table A1. Energy statistics and population between 1990 and 2019, and gross domestic product (GDP) between 2000 to 2019 at the national or local levels for the capitals of countries in the Baltic Sea basin.

		NUTS1		NUTS3		
City	**NUTS1**	**Energy Efficiency [Million Tonnes of Oil Equivalent]**	**Share of Fossil Fuel in Gross Available Energy [%]**	**NUTS3**	**Population [–]**	**GDP [EUR/Capita]**
Copenhagen	Denmark	19.08 (16.79–22.26)	84.73 (64.14–99.5)	City of Copenhagen (province)	716,243 (648,889–784,618)	60,605 (46,300–74,300)
Berlin	Germany	313.52 (285.24–332.75)	83.649 (80.02–87.72)	Berlin (district)	3,432,013 (3,278,346–3,644,826)	31,810 (25,900–43,100)
Helsinki	Finland	32.07 (25.58–36.67)	55.93 (42.79–63.83)	Helsinki-Uusimaa (region)	1,439,831 (1,219,864–1,671,024)	46,720 (36,300–56,800)
Oslo	Norway	24.99 (19.02–31.0)	56.66 (51.98–62.04)	Oslo (county)	609,141 (529,846–681,067)	94,958 (76,700–104,700)
Riga	Latvia	4.71 (3.79–7.87)	67.43 (59.83–83.94)	Riga (statistical region)	679,524 (632,614–753,006)	15,760 (6100–26,000)
Stockholm	Sweden	47.15 (43.06–50.47)	37.68 (30.29–41.14)	Stockholm County (county)	2,029,720 (1,803,377–2,344,124)	55,725 (42,300–65,700)
Tallinn	Estonia	5.64 (4.33–10.49)	91.0 (73.24–103.79)	Northern Estonia (group of counties)	557,428 (532,800–599,478)	17,350 (6600–28,600)
Vilnius	Lithuania	8.0 (5.75–16.15)	63.94 (52.48–77.94)	Vilnius County (county)	822,094 (805,173–850,668)	14,090 (4900–25,500)
Warsaw	Poland	93.37 (84.85–104.06)	94.5 (87.18–98.89)	City of Warsaw (subregion)	1,686,517 (1,618,468–1,775,986)	25,795 (13,900–41,000)

NUTS–nomenclature of territorial units for statistics. GDP–gross domestic product. Values are shown as mean, and minimum–maximum in parenthesis. Values of population refer to the time range 2007–2019 for the City of Copenhagen, 2005–2019 for Oslo, 2001–2019 for Riga and Vilnius County, and 2000–2019 for Berlin, Stockholm County, and Northern Estonia. Values of GDP refer to the time range 2008–2019 for Oslo. Own elaboration based on data from EUROSTAT (https://ec.europa.eu/eurostat, accessed on 22 January 2023).

Table A2. Coefficients of the linear fit y = a + bx, R^2, *p*-value, and rate of variation of anthropogenic emissions of SO_2, black and organic carbon for the capitals of countries in the Baltic Sea basin from 1989 to 2019.

City	SO_2 anthropogenic emissions [kg m^{-2} s^{-1}]				Rate of variation [kg m^{-2} s^{-1} $year^{-1}$] × 10^{-2}
	a	b	R^2	*p*-value	
Berlin	3.59×10^{-8}	-1.78×10^{-11}	0.68	0.0000	−2.5
Copenhagen	1.75×10^{-8}	-8.62×10^{-12}	0.78	0.0000	−2.5
Helsinki	9.1×10^{-9}	-4.41×10^{-12}	0.81	0.0000	−1.3
Oslo	1.16×10^{-9}	-4.94×10^{-13}	0.15	0.0314	−0.6
Riga	1.65×10^{-8}	-8.22×10^{-12}	0.64	0.0000	−3.1
Stockholm	3.34×10^{-8}	-1.64×10^{-11}	0.88	0.0000	−1.6
Tallinn	1.53×10^{-8}	-7.56×10^{-12}	0.54	0.0000	−2.8
Vilnius	1.46×10^{-8}	-7.25×10^{-12}	0.61	0.0000	−3.1
Warsaw	3.04×10^{-8}	-1.50×10^{-11}	0.89	0.0000	−2.0
City	BC anthropogenic emissions [kg m^{-2} s^{-1}]				Rate of variation [kg m^{-2} s^{-1} $year^{-1}$] × 10^{-2}
	a	b	R^2	*p*-value	
Berlin	-1.27×10^{-11}	9.22×10^{-15}	0.14	0.0378	−0.2
Copenhagen	-2.16×10^{-11}	1.27×10^{-14}	0.46	0.0000	0.0
Helsinki	2.88×10^{-11}	-1.30×10^{-14}	0.19	0.0131	−0.9
Oslo	-7.30×10^{-12}	4.84×10^{-15}	0.23	0.0071	−0.1
Riga	1.13×10^{-10}	-5.55×10^{-14}	0.46	0.0000	−2.4
Stockholm	-5.57×10^{-12}	3.70×10^{-15}	0.22	0.0074	−0.1
Tallinn	7.29×10^{-11}	-3.54×10^{-14}	0.4	0.0001	−1.7
Vilnius	1.01×10^{-10}	-4.96×10^{-14}	0.46	0.0000	−2.4
Warsaw	1.57×10^{-10}	-7.45×10^{-14}	0.32	0.0000	−1.4
City	OC anthropogenic emissions [kg m^{-2} s^{-1}]				Rate of variation [kg m^{-2} s^{-1} $year^{-1}$] × 10^{-2}
	a	b	R^2	*p*-value	
Berlin	3.11×10^{-11}	-1.30×10^{-14}	0.29	0.0017	−0.4
Copenhagen	-1.77×10^{-11}	1.22×10^{-14}	0.29	0.0017	0.0
Helsinki	1.31×10^{-10}	-6.21×10^{-14}	0.45	0.0000	−1.0
Oslo	2.25×10^{-11}	-8.77×10^{-15}	0.2	0.0118	−0.3
Riga	5.83×10^{-10}	-2.87×10^{-13}	0.53	0.0000	−2.3
Stockholm	2.10×10^{-11}	-8.27×10^{-15}	0.2	0.0089	−0.3
Tallinn	3.23×10^{-10}	-1.58×10^{-13}	0.51	0.0000	−1.9
Vilnius	3.08×10^{-10}	-1.52×10^{-13}	0.53	0.0000	−2.3
Warsaw	3.72×10^{-10}	-1.78×10^{-13}	0.46	0.0000	−0.9

For each city, n = 31.

Table A3. Coefficients of the linear fit y = a + bx, R^2, *p*-value, and rate of variation for the main aerosol species and total AOD over the capitals of countries in the Baltic Sea basin from 1989 to 2019.

City	Total AOD				Rate of variation [total AOD $year^{-1}$] × 10^{-3}
	a	b	R^2	*p*-value	
Berlin	4.75	−0.0023	0.54	0.0000	−3.3
Copenhagen	3.94	−0.0019	0.51	0.0000	−1.8
Helsinki	5.18	−0.0025	0.49	0.0000	−3.5
Oslo	2.02	−0.0010	0.29	0.0033	−0.4
Riga	5.78	−0.0028	0.54	0.0000	−3.9
Stockholm	4.08	−0.0020	0.55	0.0000	−2.4
Tallinn	5.07	−0.0025	0.50	0.0000	−3.4
Vilnius	5.97	−0.0029	0.55	0.0000	−4.5
Warsaw	6.11	−0.0029	0.60	0.0000	−4.6
City	SO_4 AOD				Rate of variation [SO_4 AOD $year^{-1}$] × 10^{-3}
	a	b	R^2	*p*-value	
Berlin	5.29	−0.0026	0.70	0.0000	−3.3
Copenhagen	4.52	−0.0022	0.69	0.0000	−2.1
Helsinki	4.37	−0.0021	0.62	0.0000	−2.7
Oslo	2.63	−0.0013	0.49	0.0000	−0.8
Riga	5.22	−0.0026	0.68	0.0000	−3.4
Stockholm	4.05	−0.0020	0.71	0.0000	−1.9
Tallinn	4.54	−0.0022	0.63	0.0000	−2.8
Vilnius	5.96	−0.0029	0.72	0.0000	−4.0
Warsaw	6.37	−0.0031	0.73	0.0000	−4.2
City	BC AOD				Rate of variation [BC AOD $year^{-1}$] × 10^{-5}
	a	b	R^2	*p*-value	
Berlin	−0.174	0.0001	0.40	0.0003	3.3
Copenhagen	−0.158	0.0001	0.44	0.0001	6.4
Helsinki	0.007	–	–	0.0000	–
Oslo	−0.121	0.0001	0.50	0.0000	6.7
Riga	0.0076	–	–	0.0000	–
Stockholm	−0.101	0.0001	0.31	0.0022	4.2
Tallinn	0.007	–	–	0.0000	–
Vilnius	0.008	–	–	0.0000	–
Warsaw	0.011	–	–	0.0000	–
City	OC AOD				Rate of variation [OC AOD $year^{-1}$] × 10^{-4}
	a	b	R^2	*p*-value	
Berlin	−0.511	0.0003	0.28	0.0038	1.2
Copenhagen	−0.510	0.0003	0.31	0.0022	2.3
Helsinki	0.023	–	–	0.0000	–
Oslo	−0.536	0.0003	0.40	0.0003	3.2
Riga	0.0236	–	–	0.0000	–
Stockholm	0.0193	–	–	0.0000	–
Tallinn	0.0218	–	–	0.0000	–
Vilnius	0.0249	–	–	0.0000	–
Warsaw	0.026	–	–	0.0000	–

Values relative to the time range 1991–1993 were excluded. For each city, n = 28.

Table A4. Coefficients of the linear fit y = a + bx, R2, *p*-value, and rate of variation for the percentage contribution of the main aerosol species to total AOD over the capitals of countries in the Baltic Sea basin from 1989 to 2019.

City	SO_4 AOD [%]				Rate of variation in SO_4 AOD [% year^{-1}]
	a	b	R^2	*p*-value	
Berlin	1250.4	−0.5927	0.76	0.0000	0.6
Copenhagen	1356.8	−0.6486	0.78	0.0000	0.6
Helsinki	963.73	−0.4524	0.53	0.0000	0.4
Oslo	1241.1	−0.5905	0.67	0.0000	0.4
Riga	1090.7	−0.5146	0.64	0.0000	0.6
Stockholm	1311.8	−0.6259	0.77	0.0000	0.5
Tallinn	1082.8	−0.5115	0.62	0.0000	0.5
Vilnius	1197.8	−0.5663	0.76	0.0000	0.5
Warsaw	1160.7	−0.5468	0.61	0.0000	0.5
City	BC AOD [%]				Rate of variation in BC AOD [% year^{-1}]
	a	b	R^2	*p*-value	
Berlin	−227.3	0.1163	0.85	0.0000	0.1
Copenhagen	−199.3	0.1020	0.80	0.0000	0.1
Helsinki	−147.9	0.0761	0.73	0.0000	0.1
Oslo	−177.3	0.0910	0.74	0.0000	0.1
Riga	−164.3	0.0843	0.73	0.0000	0.1
Stockholm	−176.8	0.0905	0.79	0.0000	0.1
Tallinn	−157.0	0.0806	0.73	0.0000	0.1
Vilnius	−167.4	0.0859	0.74	0.0000	0.1
Warsaw	−179.0	0.0920	0.77	0.0000	0.1
City	OC AOD [%]				Rate of variation in OC AOD [% year^{-1}]
	a	b	R^2	*p*-value	
Berlin	−574.1	0.2923	0.76	0.0000	0.3
Copenhagen	−571.7	0.2911	0.74	0.0000	0.2
Helsinki	14.77	–	–	0.0000	–
Oslo	−705.9	0.3600	0.71	0.0000	0.3
Riga	−375.7	0.1946	0.20	0.0166	0.2
Stockholm	−562.8	0.2876	0.63	0.0000	0.3
Tallinn	−316.1	0.1650	0.17	0.0300	0.2
Vilnius	−521.5	0.2671	0.42	0.0002	0.2
Warsaw	−479.7	0.2457	0.61	0.0000	0.2
City	SS AOD [%]				Rate of variation in SS AOD [% year^{-1}]
	a	b	R^2	*p*-value	
Berlin	−136.2	0.0717	0.21	0.0137	0.1
Copenhagen	−266.3	0.1402	0.25	0.0074	0.1
Helsinki	−323.1	0.1672	0.30	0.0025	0.2
Oslo	9.59	–	–	0.0000	–
Riga	−186.7	0.0977	0.17	0.0307	0.2
Stockholm	−288.7	0.1506	0.39	0.0004	0.1
Tallinn	−269.4	0.1398	0.73	0.0000	0.1
Vilnius	5.70	–	–	0.0000	–
Warsaw	−91.3	0.0477	0.23	0.0092	0.1

Table A4. *Cont.*

City	DU AOD [%]				Rate of variation in DU AOD [% year^{-1}]
	a	b	R^2	*p*-value	
Berlin	12.35	–	–	0.0000	0.0
Copenhagen	−219.6	0.1153	0.18	0.0237	0.1
Helsinki	−220.0	0.1156	0.14	0.0469	0.1
Oslo	12.29	–	–	0.0000	–
Riga	−264.0	0.1380	0.22	0.0129	0.1
Stockholm	11.53	–	–	0.0000	–
Tallinn	−240.36	0.1261	0.16	0.0323	0.1
Vilnius	−317.4	0.1649	0.28	0.0040	0.1
Warsaw	−310.8	0.1613	0.23	0.0101	0.2

Values relative to the time range 1991–1993 were excluded. For each city, n = 28.

Table A5. Percentage contribution of the main aerosol species of anthropogenic and natural origins to total aerosol optical depth (AOD) from 1989 to 2019, and trend in anthropogenic and natural AOD percentage contributions to total AOD from 1989 to 2008.

City	**Natural AOD [%]**	**Anthropogenic AOD [%]**	**Trend in AOD Percentage Contribution to Total AOD from 1989 to 2008**					
			Anthropogenic AOD			**Natural AOD**		
	Mean (Min–Max)	**Mean (Min–Max)**	**R^2**	***p*-Value**	**Rate of Variation [% Year^{-1}]**	**R^2**	***p*-Value**	**Rate of Variation [% Year^{-1}]**
Berlin	20.0 (13.9–25.7)	80.0 (74.3–86.1)	0.86	9.72×10^{-8}	−0.6	0.86	9.72×10^{-8}	0.6
Copenhagen	26.4 (19.7–33.6)	73.6 (66.4–80.3)	0.73	1.14×10^{-5}	−0.7	0.73	1.14×10^{-5}	0.7
Helsinki	24.1 (14.6–29.7)	75.9 (70.3–85.4)	0.77	4.25×10^{-6}	−0.6	0.77	4.25×10^{-6}	0.6
Oslo	21.9 (13.2–27.4)	78.1 (72.6–86.8)	0.6	0.0003	−0.4	0.6	0.0003	0.4
Riga	22.1 (13.8–27.6)	77.9 (72.4–86.2)	0.78	2.65×10^{-6}	−0.6	0.78	2.65×10^{-6}	0.6
Stockholm	24.8 (16.0–29.3)	75.2 (70.7–84.0)	0.73	1.43×10^{-5}	−0.5	0.73	1.43×10^{-5}	0.5
Tallinn	23.4 (14.6–28.8)	76.6 (71.2–85.4)	0.76	5.2×10^{-6}	−0.6	0.76	5.2×10^{-6}	0.6
Vilnius	19.0 (10.8–24.9)	81.0 (75.0–89.2)	0.86	8.52×10^{-8}	−0.6	0.86	8.52×10^{-8}	0.6
Warsaw	17.2 (9.7–23.5)	82.8 (76.5–90.3)	0.88	2.85×10^{-8}	−0.7	0.86	9.72×10^{-8}	0.7

Values relative to the time range 1991–1993 were excluded. For each city, n = 28.

Table A6. Coefficients of the linear fit y = a + bx, R^2, *p*-value, number of observations (n) for the response variables (i.e., total and SO_4 AOD) and the independent variables [i.e., annual data of gross domestic product (GDP), and share of fossil fuel in gross available energy (SFFGAE)] over the capitals of countries in the Baltic Sea basin from 2000 to 2019.

City	n	y	a	b	x [Unit of Measurement]	R^2	*p*-Value
Berlin	20	Total AOD	3.30	−0.0016	Time [year]	0.40	0.0027
	20	SO_4 AOD	2.98	−0.0014	Time [year]	0.55	0.0002
Helsinki	20	SO_4 AOD	0.031	0.0008	SFFGAE [%]	0.26	0.0211
Oslo	12	SO_4 AOD	0.120	-6.4641×10^{-7}	GDP [EUR/capita]	0.39	0.0292
Stockholm	20	Tot AOD	0.060	0.0020	SFFGAE [%]	0.34	0.0075
	20	SO_4 AOD	0.117	-8.196×10^{-7}	GDP [EUR/capita]	0.51	0.0004
Tallinn	20	SO_4 AOD	0.088	-8.205×10^{-7}	GDP [EUR/capita]	0.31	0.011
Vilnius	19	SO_4 AOD	0.118	-1.3768×10^{-6}	GDP [EUR/capita]	0.70	0.0000
Warsaw	20	Total AOD	3.67	−0.0017	Time [year]	0.58	0.0001
	20	SO_4 AOD	3.29	−0.0016	Time [year]	0.67	0.0000

SFFGAE is at nomenclature of territorial units for statistics (NUTS) level 1 level; GDP is at NUTS3 level; Population is at NUTS3 level. Time span is for Oslo 2005– 2019, and 2001–2019 for Vilnius and Riga.

References

1. Provençal, S.; Kishcha, P.; da Silva, A.M.; Elhacham, E.; Alpert, P. AOD distributions and trends of major aerosol species over a selection of the world's most populated cities based on the 1st version of NASA's MERRA Aerosol Reanalysis. *Urban Clim.* **2017**, *20*, 168–191. [CrossRef] [PubMed]
2. Rizza, U.; Mancinelli, E.; Morichetti, M.; Passerini, G.; Virgili, S. Aerosol Optical Depth of the Main Aerosol Species over Italian Cities Based on the NASA/MERRA-2 Model Reanalysis. *Atmosphere* **2019**, *10*, 709. [CrossRef]
3. Mehta, M.; Singh, N.; Anshumali. Global trends of columnar and vertically distributed properties of aerosols with emphasis on dust, polluted dust and smoke—Inferences from 10-year long CALIOP observations. *Remote Sens. Environ.* **2018**, *208*, 120–132. [CrossRef]
4. Mehta, M.; Singh, R.; Singh, A.; Singh, N. Recent global aerosol optical depth variations and trends—A comparative study using MODIS and MISR level 3 datasets. *Remote Sens. Environ.* **2016**, *181*, 137–150. [CrossRef]
5. Filonchyk, M.; Hurynovich, V.; Yan, H. Trends in aerosol optical properties over Eastern Europe based on MODIS-Aqua. *Geosci. Front.* **2020**, *11*, 2169–2181. [CrossRef]
6. Filonchyk, M.; Hurynovich, V.; Yan, H.; Zhou, L.; Gusev, A. Climatology of aerosol optical depth over Eastern Europe based on 19 years (2000–2018) MODIS TERRA data. *Int. J. Climatol.* **2020**, *40*, 3531–3549. [CrossRef]
7. Di Antonio, L.; Di Biagio, C.; Foret, G.; Formenti, P.; Siour, G.; Doussin, J.F.; Beekmann, M. Aerosol optical depth climatology from the high–resolution MAIAC product over Europe: Differences between major European cities and their surrounding environments. *Atmos. Chem. Phys.* **2023**, *23*, 12455–12475. [CrossRef]
8. Gupta, G.; Ratnam, M.V.; Madhavan, B.L.; Narayanamurthy, C.S. Long-term trends in Aerosol Optical Depth obtained across the globe using multi-satellite measurements. *Atmos. Environ.* **2022**, *273*, 118953. [CrossRef]
9. Gupta, G.; Ratnam, M.V.; Madhavan, B.L.; Jayaraman, A. Global trends in the aerosol optical, physical, and morphological properties obtained using multi-sensor measurements. *Atmos. Environ.* **2023**, *295*, 119569. [CrossRef]
10. Winker, D.M.; Vaughan, M.A.; Omar, A.; Hu, Y.; Powell, K.A.; Liu, Z.; Hunt, W.H.; Young, S.A. Overview of the CALIPSO Mission and CALIOP Data Processing Algorithms. *J. Atmos. Ocean. Technol.* **2009**, *26*, 2310–2323. [CrossRef]
11. Gupta, G.; Ratnam, M.V.; Madhavan, B.L. Changing patterns in the highly contributing aerosol types/species across the globe in the past two decades. *Sci. Total Environ.* **2023**, *897*, 165389. [CrossRef] [PubMed]
12. Gelaro, R.; McCarty, W.; Suárez, M.J.; Todling, R.; Molod, A.; Takacs, L.; Wargan, K. The modern-era retrospective analysis for research and applications, version 2 (MERRA-2). *J. Clim.* **2017**, *30*, 5419–5454. [CrossRef] [PubMed]
13. Rienecker, M.M.; Suarez, M.J.; Gelaro, R.; Todling, R.; Bacmeister, J.; Liu, E.; Bosilovich, M.G. MERRA: NASA's modern-era retrospective analysis for research and applications. *J. Clim.* **2011**, *24*, 3624–3648. [CrossRef]
14. Markowicz, K.M.; Stachlewska, I.S.; Zawadzka-Manko, O.; Wang, D.; Kumala, W.; Chilinski, M.T.; Makuch, P.; Markuszewski, P.; Rozwadowska, A.K.; Petelski, T.; et al. A Decade of Poland-AOD Aerosol Research Network Observations. *Atmosphere* **2021**, *12*, 1583. [CrossRef]
15. Naqvi, A. Decoupling trends of emissions across EU regions and the role of environmental policies. *J. Clean. Prod.* **2021**, *323*, 129130. [CrossRef]

16. Qin, W.; Liu, Y.; Wang, L.; Lin, A.; Xia, X.; Che, H.; Bilal, M.; Zhang, M. Characteristic and driving factors of aerosol optical depth over mainland China during 1980–2017. *Remote Sens.* **2018**, *10*, 1064. [CrossRef]
17. Papachristopoulou, K.; Raptis, I.P.; Gkikas, A.; Fountoulakis, I.; Masoom, A.; Kazadzis, S. Aerosol optical depth regime over megacities of the world. *Atmos. Chem. Phys.* **2022**, *22*, 15703–15727. [CrossRef]
18. Lyapustin, A.; Wang, Y.J.; Korkin, S.; Huang, D. MODIS Collection 6 MAIAC algorithm. *Atmos. Meas. Tech.* **2018**, *11*, 5741–5765. [CrossRef]
19. Remer, L.A.; Kaufman, Y.J.; Tanre, D.; Mattoo, S.; Chu, D.A.; Martins, J.V.; Li, R.R.; Ichoku, C.; Levy, R.C.; Kleidman, R.G.; et al. The MODIS aerosol algorithm, products, and validation. *J. Atmos. Sci.* **2005**, *62*, 947–973. [CrossRef]
20. Levy, R.C.; Remer, L.A.; Mattoo, S.; Vermote, E.F.; Kaufman, Y.J. Second-generation operational algorithm: Retrieval of aerosol properties over land from inversion of Moderate Resolution Imaging Spectroradiometer spectral reflectance. *J. Geophys. Res. Atmos.* **2007**, *112*, D13211. [CrossRef]
21. European Commission. Commission Delegated Regulation 2019/1755 of 8 August 2019 amending the Annexes to Regulation (EC) No 1059/2003 of the European Parliament and of the Council on the Establishment of a Common Classification of Territorial Units for Statistics (NUTS). C/2019/5841. Document 32019R1755. 2019. Available online: http://data.europa.eu/eli/reg_del/2019/1755/oj (accessed on 22 January 2024).
22. Purvins, A.; Fulli, G.; Covrig, C.-F.; Chaouachi, A.; Bompard, E.; Carpaneto, E.; Huang, T.; Pi, R.J.; Mutule, A.; Oleinikova, I.; et al. *The Baltic Power System between East and West Interconnections*; Publications Office of the European Union: Luxembourg, 2016; Available online: https://data.europa.eu/doi/10.2790/411653 (accessed on 8 May 2024).
23. Štreimikienė, D.; Balezentis, T. Kaya identity for analysis of the main drivers of GHG emissions and feasibility to implement EU "20–20–20" targets in the Baltic States. *Renew. Sustain. Energy Rev.* **2016**, *58*, 1108–1113. [CrossRef]
24. Rienecker, M.; Suarez, M.; Todling, R.; Bacmeister, J.; Takacs, L.; Liu, H.-C.; Gu, W.; Sienkiewicz, M.; Koster, R.; Gelaro, R. *The GEOS-5 Data Assimilation System—Documentation of Versions 5.0.1, 5.1.0, and 5.2.0*; Technical Report Series on Global Modeling and Data Assimilation; NASA: Washington, DC, USA, 2008.
25. Molod, A.; Takacs, L.; Suarez, M.; Bacmeister, J.; Song, I.-S.; Eichmann, A. *The GEOS-5 Atmospheric General Circulation Model: Mean Climate and Development from MERRA to Fortuna*; NASA: Washington, DC, USA, 2012.
26. Wu, W.-S.; Purser, R.J.; Parrish, D.F. Three-dimensional variational analysis with spatially inhomogeneous covariances. *Mon. Wea. Rev.* **2002**, *130*, 2905–2916. [CrossRef]
27. Kleist, D.T.; Parrish, D.F.; Derber, J.C.; Treadon, R.; Wu, W.-S.; Lord, S. Introduction of the GSI into the NCEP Global Data Assimilation System. *Weather Forecast.* **2009**, *24*, 1691–1705. [CrossRef]
28. Putman, W.M.; Lin, S.J. Finite-volume transport on various cubed-sphere grids. *J. Comput. Phys.* **2007**, *227*, 55–78. [CrossRef]
29. Chin, M.; Ginoux, P.; Kinne, S.; Torres, O.; Holben, B.N.; Duncan, B.N.; Martin, R.V.; Logan, J.A.; Higurashi, A.; Nakajima, T. Tropospheric aerosol optical thickness from the GOCART model and comparisons with satellite and Sun photometer measurements. *J. Atmos. Sci.* **2002**, *59*, 461–483. [CrossRef]
30. Colarco, P.; da Silva, A.; Chin, M.; Diehl, T. Online simulations of global aerosol distributions in the NASA GEOS-4 model and comparisons to satellite and ground-based aerosol optical depth. *J. Geophys. Res. Atmos.* **2010**. [CrossRef]
31. Heidinger, A.K.; Cao, C.; Sullivan, J.T. Using Moderate Resolution Imaging Spectrometer (MODIS) to calibrate Advanced Very High Resolution Radiometer reflectance channels. *J. Geophys. Res.* **2002**, *107*, 4702. [CrossRef]
32. Kahn, R.A.; Gaitley, B.J.; Martonchik, J.V.; Diner, D.J.; Crean, K.A.; Holben, B. Multiangle Imaging Spectroradiometer (MISR) global aerosol optical depth validation based on 2 years of coincident Aerosol Robotic Network (AERONET) observations. *J. Geophys. Res. Atmos.* **2005**, *110*, D10S04. [CrossRef]
33. Holben, B.N.; Eck, T.F.; Slutsker, I.; Tanré, D.; Buis, J.P.; Setzer, A.; Vermote, E.; Reagan, J.A.; Kaufman, Y.J.; Nakajima, T.; et al. AERONET—A Federated Instrument Network and Data Archive for Aerosol Characterization. *Remote Sens. Environ.* **1998**, *66*, 1–16. [CrossRef]
34. Lacima, A.; Petetin, H.; Soret, A.; Bowdalo, D.; Jorba, O.; Chen, Z.; Méndez Turrubiates, R.F.; Achebak, H.; Ballester, J.; Pérez García-Pando, C. Long-term evaluation of surface air pollution in CAMSRA and MERRA-2 global reanalyses over Europe (2003–2020). *Geosci. Model Dev.* **2023**, *16*, 2689–2718. [CrossRef]
35. Diehl, T.; Heil, A.; Chin, M.; Pan, X.; Streets, D.; Schultz, M.; Kinne, S. Anthropogenic, biomass burning, and volcanic emissions of black carbon, organic carbon, and SO2 from 1980 to 2010 for hindcast model experiments. *Atmos. Chem. Phys. Discuss.* **2012**, *12*, 24895–24954. [CrossRef]
36. Janssens-Maenhout, G.; Crippa, M.; Guizzardi, D.; Muntean, M.; Schaaf, E. Joint Research Centre Data Catalogue—Emissions Database for Global Atmospheric Research, version v4.2 (time-series). European Commission, Joint Research Centre (JRC) [data set]. Available online: http://data.europa.eu/89h/jrc-edgar-emissiontimeseriesv42 (accessed on 9 May 2024).
37. Janssens-Maenhout, G. Joint Research Centre Data Catalogue—EDGARv4.2 Emission Maps. European Commission, Joint Research Centre (JRC) [data set]. Available online: http://data.europa.eu/89h/jrc-edgar-emissionmapsv42 (accessed on 9 May 2024).
38. Duncan, B.N.; Martin, R.V.; Staudt, A.C.; Yevich, R.; Logan, J.A. Interannual and seasonal variability of biomass burning emissions constrained by satellite observations. *J. Geophys. Res. Atmos.* **2003**, *108*, ACH-1. [CrossRef]
39. Randerson, J.T.; Liu, H.; Flanner, M.G.; Chambers, S.D.; Jin, Y.; Hess, P.G.; Pfister, G.; Mack, M.C.; Treseder, K.K.; Welp, L.R.; et al. The impact of boreal forest fire on climate warming. *Science* **2006**, *314*, 1130–1133. [CrossRef] [PubMed]

40. van der Werf, G.R.; Randerson, J.T.; Giglio, L.; Collatz, G.J.; Kasibhatla, P.S.; Arellano, A.F., Jr. Interannual variability in global biomass burning emissions from 1997 to 2004. *Atmos. Chem. Phys.* **2006**, *6*, 3423–3441. [CrossRef]
41. Darmenov, A.; Silva, A. *The Quick Fire Emissions Dataset (QFED): Documentation of Versions 2.1, 2.2 and 2.4*; Technical Report Series on Global Modeling and Data Assimilation; NASA: Washington, DC, USA, 2015; Volume 38. Available online: http://gmao.gsfc.nasa.gov/pubs/docs/Darmenov796.pdf (accessed on 4 September 2023).
42. Guenther, A.; Hewitt, C.N.; Erickson, D.; Fall, R.; Geron, C.; Graedel, T.; Harley, P.; Klinger, L.; Lerdau, M.; Mckay, W.A.; et al. A global model of natural volatile organic compound emissions. *J. Geophys. Res. Atmos.* **1995**, *100*, 8873–8892. [CrossRef]
43. Randles, C.A.; da Silva, A.; Buchard, V.; Colarco, P.R.; Darmenov, A.S.; Govindaraju, R.C.; Smirnov, A.; Ferrare, R.A.; Hair, J.W.; Shinozuka, Y.; et al. The MERRA-2 Aerosol Reanalysis, 1980-onward, Part I: System Description and Data Assimilation Evaluation. *J. Clim.* **2017**, *30*, 6823–6850. [CrossRef] [PubMed]
44. Randles, C.A.; da Silva, A.M.; Buchard, V.; Darmenov, A.; Colarco, P.R.; Aquila, V.; Bian, H.; Nowottnick, E.P.; Pan, X.; Smirnov, A.; et al. *The MERRA-2 Aerosol Assimilation*; NASA Technical Report Series on Global Modeling and Data Assimilation; NASA: Washington, DC, USA, 2016; Volume 45, p. 143.
45. Crippa, M.; Guizzardi, D.; Muntean, M.; Schaaf, E.; Dentener, F.; Van Aardenne, J.A.; Monni, S.; Doering, U.; Olivier, J.G.; Pagliari, V.; et al. Gridded emissions of air pollutants for the period 1970–2012 within EDGAR v4.3.2. *Earth Syst. Sci. Data* **2018**, *10*, 1987–2013. [CrossRef]
46. Eyring, V.; Köhler, H.W.; van Aardenne, J.; Lauer, A. Emissions from international shipping: 1. The last 50 years. *J. Geophys. Res. Atmos.* **2005**, *110*, D17305. [CrossRef]
47. Marticorena, B.; Bergametti, G. Modeling the atmospheric dust cycle: 1. Design of a soil-derived dust emission scheme. *J. Geophys. Res. Atmos.* **1995**, *100*, 16415–16430. [CrossRef]
48. Gong, S.L. A parameterization of sea-salt aerosol source function for sub- and super-micron particles. *Glob. Biogeochem. Cycles* **2003**, *17*, 1097. [CrossRef]
49. Jaeglé, L.; Quinn, P.K.; Bates, T.S.; Alexander, B.; Lin, J.-T. Global distribution of sea salt aerosols: New constraints from in situ and remote sensing observations. *Atmos. Chem. Phys.* **2011**, *11*, 3137–3157. [CrossRef]
50. Hsu, N.C.; Herman, J.R.; Bhartia, P.K.; Seftor, C.J.; Torres, O.; Thompson, A.M.; Gleason, J.F.; Eck, T.F.; Holben, B.N. Detection of biomass burning smoke from TOMS measurements. *Geophys. Res. Lett.* **1996**, *23*, 745–748. [CrossRef]
51. Arino, O.; Simon, M.; Piccolini, I.; Rosaz, J.-M. The ERS-2 ATSR-2 World Fire Atlas and the ERS-2 ATSR-2 World Burnt Surface Atlas Projects. In Proceedings of the 8th ISPRS Conference on Physical Measurement & Signatures in Remote Sensing, Aussois, France, 8–12 January 2001.
52. Giglio, L.; Schroeder, W.; Justice, C.O. The Collection 6 MODIS Active Fire Detection Algorithm and Fire Products. *Remote Sens. Environ.* **2016**, *178*, 31–41. [CrossRef] [PubMed]
53. Justice, C.O.; Townshend, J.R.G.; Vermote, E.F.; Masuoka, E.; Wolfe, R.E.; Saleous, N.; Roy, D.P.; Morisette, J.T. An overview of MODIS Land data processing and product status. *Remote Sens. Environ* **2002**, *83*, 3–15. [CrossRef]
54. Hsu, N.C.; Tsay, S.C.; King, M.D.; Herman, J.R. Aerosol properties over bright-reflecting source regions. *IEEE Trans. Geosci. Remote Sens.* **2004**, *42*, 557–569. [CrossRef]
55. Levy, R.C.; Mattoo, S.; Munchak, L.A.; Remer, L.A.; Sayer, A.M.; Patadia, F.; Hsu, N.C. The Collection 6 MODIS aerosol products over land and ocean. *Atmos. Meas. Tech.* **2013**, *6*, 2989. [CrossRef]
56. Sayer, A.M.; Munchak, L.A.; Hsu, N.C.; Levy, R.C.; Bettenhausen, C.; Jeong, M.-J. MODIS Collection 6 aerosol products: Comparison between Aqua's e-Deep Blue, Dark Target, and "merged" data sets, and usage recommendations. *J. Geophys. Res. Atmos.* **2014**, *119*, 13965–13989. [CrossRef]
57. Diner, D.J.; Beckert, J.C.; Reilly, T.H.; Bruegge, C.J.; Conel, J.E.; Kahn, R.A.; Martonchik, J.V.; Ackerman, T.P.; Davies, R.; Gerstl, S.A.; et al. Multi-angle Imaging SpectroRadiometer (MISR) instrument description and experiment overview. *IEEE Trans. Geosci. Remote Sens.* **1998**, *36*, 1072–1087. [CrossRef]
58. Mancinelli, E.; Canestrari, F.; Graziani, A.; Rizza, U.; Passerini, G. Sustainable Performances of Small to Medium-Sized Airports in the Adriatic Region. *Sustainability* **2021**, *13*, 13156. [CrossRef]
59. Smith, G. Step away from stepwise. *J. Big Data* **2018**, *5*, 32. [CrossRef]
60. Draper, N.R.; Smith, H. *Applied Regression Analysis*; John Wiley & Sons: Hoboken, NJ, USA, 1998; Volume 326, pp. 307–312.
61. Yang, Y.; Lou, S.; Wang, H.; Wang, P.; Liao, H. Trends and source apportionment of aerosols in Europe during 1980–2018. *Atmos. Chem. Phys.* **2020**, *20*, 2579–2590. [CrossRef]
62. Saponaro, G.; Kolmonen, P.; Sogacheva, L.; Rodriguez, E.; Virtanen, T.; de Leeuw, G. Estimates of the aerosol indirect effect over the Baltic Sea region derived from 12 years of MODIS observations. *Atmos. Chem. Phys.* **2017**, *17*, 3133–3143. [CrossRef]
63. Zhao, B.; Jiang, J.H.; Diner, D.J.; Su, H.; Gu, Y.; Liou, K.-N.; Jiang, Z.; Huang, L.; Takano, Y.; Fan, X. Intra-annual variations of regional aerosol optical depth, vertical distribution, and particle types from multiple satellite and ground-based observational datasets. *Atmos. Chem. Phys.* **2018**, *18*, 11247–11260. [CrossRef]
64. Ansmann, A.; Mattis, I.; Wandinger, U.; Wagner, F.; Reichardt, J.; Deshler, T. Evolution of the Pinatubo aerosol: Raman lidar observations of particle optical depth, effective radius, mass, and surface area over Central Europe at 53.4 N. *J. Atmos. Sci.* **1997**, *54*, 2630–2641. [CrossRef]

65. Shantikumar, N.S.; Larson, E.J.; Dumka, U.C.; Estelles, V.; Campanelli, M.; Steve, C. Long-term (1995–2018) aerosol optical depth derived using ground based AERONET and SKYNET measurements from aerosol aged-background sites. *Atmos. Pollut. Res.* **2019**, *10*, 608–620. [CrossRef]
66. Sun, E.; Xu, X.; Che, H.; Tang, Z.; Gui, K.; An, L.; Lu, C.; Shi, G. Variation in MERRA-2 aerosol optical depth and absorption aerosol optical depth over China from 1980 to 2017. *J. Atmos. Sol. Terr. Phys.* **2019**, *186*, 8–19. [CrossRef]
67. Rizza, U.; Donnadieu, F.; Morichetti, M.; Avolio, E.; Castorina, G.; Semprebello, A.; Magazu, S.; Passerini, G.; Mancinelli, E.; Biensan, C. Airspace Contamination by Volcanic Ash from Sequences of Etna Paroxysms: Coupling the WRF-Chem Dispersion Model with Near-Source L-Band Radar Observations. *Remote Sens.* **2023**, *15*, 3760. [CrossRef]
68. Markowicz, K.M.; Zawadzka-Manko1, O.; Posyniak, M. A large reduction of direct aerosol cooling over Poland in the last decades. *Int. J. Climatol.* **2022**, *42*, 4129–4146. [CrossRef]
69. Logothetis, S.A.; Salamalikis, V.; Gkikas, A.; Kazadzis, S.; Amiridis, V.; Kazantzidis, A. 15-Year Variability of Desert Dust Optical Depth on Global and Regional Scales. *Atmos. Chem. Phys.* **2021**, *21*, 16499–16529. [CrossRef]